AD-A088 576 NATIONAL OCEANIC AND ATMOSPHERIC ADMINISTRATION BOUL--ETC F/G 17/9
WIND SHEAR DETECTION WITH PULSE DOPPLER RADAR.(U)
JAN 80 R G STRAUCH, W B SWEEZY

UNCLASSIFIED

DOT-FA76WAT622

FAA-RD-80-26

NL

1 OF 1
AD A
088576

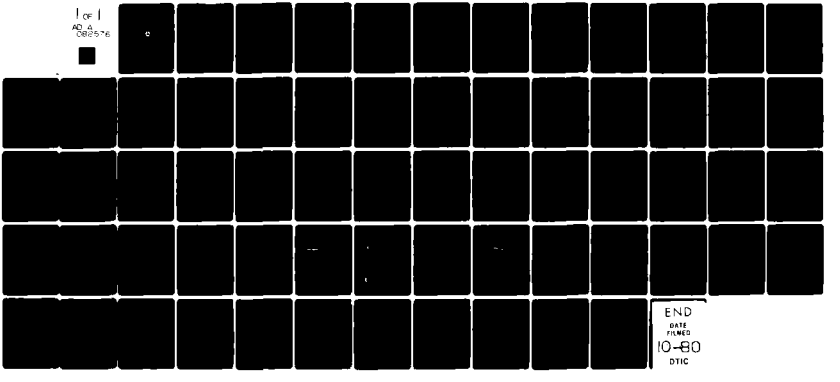

END
DATE FILMED
10-80
DTIC

Report No. FAA-RD-80-26

WIND SHEAR DETECTION WITH PULSE DOPPLER RADAR

R.G. Strauch
W.B. Sweezy

Wave Propagation Laboratory
National Oceanic and Atmospheric Administration
Boulder, Colorado 80303

January 1980
Final Report

Prepared for

U.S. DEPARTMENT OF TRANSPORTATION
FEDERAL AVIATION ADMINISTRATION
Systems Research & Development Service
Washington, D.C. 20590

NOTICE

This document is disseminated under the sponsorship of the Department of Transportation in the interest of information exchange. The United States Government assumes no liability for the contents or use thereof.

Technical Report Documentation Page

1. Report No.	2. Government Accession No.	3. Recipient's Catalog No.
FAA-RD-80-26	AD-A088 526	

4. Title and Subtitle	5. Report Date
WIND SHEAR DETECTION WITH PULSE DOPPLER RADAR,	January 1980
	6. Performing Organization Code
	8. Performing Organization Report No.

7. Author(s)	
R. G. Strauch and W. B. Sweezy	

9. Performing Organization Name and Address	10. Work Unit No. (TRAIS)
Wave Propagation Laboratory National Oceanic and Atmospheric Administration Boulder, Colorado 80303	11. Contract or Grant No. DOT-FA76WAI622, Task VII

12. Sponsoring Agency Name and Address	13. Type of Report and Period Covered
U.S. Department of Transportation Federal Aviation Administration Systems Research and Development Service Washington, D.C. 20590	Final Report. September 1977 to September, 1979
	14. Sponsoring Agency Code FAA/ARD - 231

15. Supplementary Notes

16. Abstract

Measurement of wind profiles and wind shear near air terminals in all weather regimes may be possible with pulse Doppler radar. The use of radar for solving the airport wind shear problem was investigated experimentally and with computer simulations. Radar tests are continuing. A single Doppler device cannot measure the complex three-dimensional wind field that exists in some weather events. In Phase I of this project a computer simulation showed that a radar with a 150 m pulse length and a 1.5 degree beamwidth could resolve low level wind profiles. The computer simulation program has been expanded so that the radar measured radial velocity profile and the field of radial velocities could be calculated and displayed for any analytic or numerical input wind model. Various output displays are available. Both the location of the radar and the volume that is scanned can be chosen relative to the input coordinate system. The program can also accept input wind models expressed relative to the approach path. Effects of antenna beamwidth and radar range resolution can be simulated. The program is useful for studying the expected observations for any radar (or laser) Doppler system. Radar reflectivity is assumed constant but the program could readily accommodate reflectivity gradients. Thus the program should prove valuable for studying the utility of single Doppler radar observations in any situation.

The simulation results, using wind models that can cause problems for landing aircraft, show that the radial velocity field of a single Doppler radar depicts wind shear by a change in the orientation of contours of constant velocity.

17. Key Words	18. Distribution Statement
Wind shear, Doppler radar, Aircraft safety, Wind profiles and Severe weather.	Document is available to the U.S. public through the National Technical Information Service, Springfield, Virginia 22161.

19. Security Classif. (of this report)	20. Security Classif. (of this page)	21. No. of Pages	22. Price
Unclassified	Unclassified	60	

Form DOT F 1700.7 (8-72) Reproduction of completed page authorized

METRIC CONVERSION FACTORS

Approximate Conversions to Metric Measures

Symbol	When You Know	Multiply by	To Find	Symbol
	LENGTH			
in	inches	*2.5	centimeters	cm
ft	feet	30	centimeters	cm
yd	yards	0.9	meters	m
mi	miles	1.6	kilometers	km
	AREA			
in^2	square inches	6.5	square centimeters	cm^2
ft^2	square feet	0.09	square meters	m^2
yd^2	square yards	0.8	square meters	m^2
mi^2	square miles	2.6	square kilometers	km^2
	acres	0.4	hectares	ha
	MASS (weight)			
oz	ounces	28	grams	g
lb	pounds	0.45	kilograms	kg
	short tons (2000 lb)	0.9	tonnes	t
	VOLUME			
tsp	teaspoons	5	milliliters	ml
Tbsp	tablespoons	15	milliliters	ml
fl oz	fluid ounces	30	milliliters	ml
c	cups	0.24	liters	l
pt	pints	0.47	liters	l
qt	quarts	0.95	liters	l
gal	gallons	3.8	liters	l
ft^3	cubic feet	0.03	cubic meters	m^3
yd^3	cubic yards	0.76	cubic meters	m^3
	TEMPERATURE (exact)			
°F	Fahrenheit temperature	5/9 (after subtracting 32)	Celsius temperature	°C

*1 in = 2.54 (exactly). For other exact conversions and more detailed tables, see NBS Misc. Publ. 286, Units of Weights and Measures, Price $2.25, SD Catalog No. C13.10:286.

Approximate Conversions from Metric Measures

Symbol	When You Know	Multiply by	To Find	Symbol
	LENGTH			
mm	millimeters	0.04	inches	in
cm	centimeters	0.4	inches	in
m	meters	3.3	feet	ft
m	meters	1.1	yards	yd
km	kilometers	0.6	miles	mi
	AREA			
cm^2	square centimeters	0.16	square inches	in^2
m^2	square meters	1.2	square yards	yd^2
km^2	square kilometers	0.4	square miles	mi^2
ha	hectares (10,000 m^2)	2.5	acres	
	MASS (weight)			
g	grams	0.035	ounces	oz
kg	kilograms	2.2	pounds	lb
t	tonnes (1000 kg)	1.1	short tons	
	VOLUME			
ml	milliliters	0.03	fluid ounces	fl oz
l	liters	2.1	pints	pt
l	liters	1.06	quarts	qt
l	liters	0.26	gallons	gal
m^3	cubic meters	35	cubic feet	ft^3
m^3	cubic meters	1.3	cubic yards	yd^3
	TEMPERATURE (exact)			
°C	Celsius temperature	9/5 (then add 32)	Fahrenheit temperature	°F

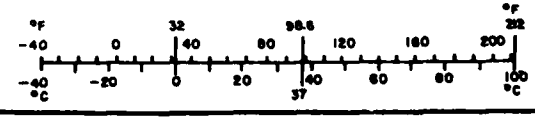

TABLE OF CONTENTS

LIST OF ILLUSTRATIONS

LIST OF TABLES

1. INTRODUCTION

During the past decade a number of costly aircraft accidents have occurred where wind shear has been identified as the probable cause[1]. The identification of a wind shear hazard for large jet aircraft taking off or on final approach has prompted the Federal Aviation Administration (FAA) to examine various ground based in-situ and remote sensing devices to determine if a wind shear warning system could be developed. Surface arrays of pressure, temperature[2], and wind sensors[3] may give indications of dangerous winds near the airport, but remote sensing devices offer the possibility of measuring dangerous winds along the actual track of the aircraft. Early research work to solve the wind shear problem with remote sensing led to the installation and test of a system for measuring wind profiles at Dulles International Airport[4]. This system used an acoustic radar for measuring vertical profiles of horizontal wind to 500 m altitude in the precipitation-free atmosphere and, during rain, when the acoustic system could not obtain data because of excessive noise, a low-power microwave radar measured wind profiles. However, measurement of the vertical profile of horizontal wind at one point near the runways can only detect those wind shear hazards that arise from vertical gradients of the horizontal wind. Hazardous winds from thunderstorm outflows, for example, may not be detected by such a system. Therefore, research work has continued to develop remote sensing techniques for observing winds along the aircraft track. Both laser radar systems[5] and microwave radar systems offer this potential.

Microwave radars have been a tool for operational meteorology for over 20 years. During the 1970's, Doppler radar technology has developed so that the next-generation of weather radars will include Doppler capability[6]. The Doppler weather radars measure the reflectivity of the hydrometeor scatterers, just as conventional or non-Doppler radars, but they also measure the average radial velocity and the spread of the radial velocities in each radar resolution cell. If the Doppler radar is sufficiently sensitive, it can measure the reflectivity and velocity from scattering in the precipitation-free atmosphere. In this case the scattering arises from refractive index variations which occur throughout the lower atmosphere and especially in the planetary boundary layer.

The radar senses that component of refractive turbulence whose scale size is one-half the radar wavelength. Typical meteorological radars with wavelengths of 5 to 20 cm have sufficient sensitivity to detect refractive turbulence in the planetary boundary layer, sometimes to a range of more than 50 km[7]. Microwave radar, therefore, offers the possibility of all-weather wind measurements to altitudes needed to insure safe operation of aircraft in the terminal area. The actual altitudes where wind shear poses a threat to aircraft depends on the aircraft response and therefore on the type of aircraft. Measurement of wind shear in the lowest 500 m has been the goal for remote sensing systems.

In January, 1977 the National Oceanic and Atmospheric Administration (NOAA) and the FAA began a joint program to examine pulse Doppler radar as a potential wind shear detection device. [NOAA's Wave Propagation Laboratory (WPL) had been involved with the Doppler radar work at Dulles and had also developed a Frequency Modulated-Continuous Wave (FM-CW) Doppler radar for wind measurements in the precipitation-free atmosphere[8]. The FM-CW radar is also being tested as a potential wind shear warning device for the United States Air Force[9]]. The objective of the joint program was to explore whether an existing FAA air traffic control radar could be configured for wind measurements. A radar wind shear warning system would be much more attractive if existing radars could be used. Experimental work was to be performed at the National Aviation Facilities Experimental Center (NAFEC) at Atlantic City, NJ. Limitations of Doppler radar were recognized from the start and some of the important limitations would be explored by actual testing at NAFEC and some by computer simulations. The radar was to be equipped with a 15 foot parabolic reflector antenna and a simple data processing system, sufficient to demonstrate the ability of radar to measure Doppler spectra in clear air, would be used. Major questions to be answered with the radar were: (a) how would ground clutter restrict the minimum range or altitude at which clear air radar signals could be measured and (b) was the radar sensitive enough to measure clear air returns under all conditions. Major questions to be answered by computer simulation were: (a) does a 15 foot diameter antenna give sufficient resolution to measure wind profiles and (b) how should the radar, which measures only one component of the wind, be used to detect and measure dangerous winds.

2. NAFEC RADAR SYSTEM AND TESTS

One channel of an ASR-8 radar has been configured for wind shear tests. Figure 2.1 shows a block diagram of the system. The 15 foot parabolic reflector was procured from the Microwave Specialty Corp. in San Diego, CA and was installed in the spring of 1978. A pedestal was not available until May, 1979 so many of the tests were conducted with a fixed antenna position. The transmitter, preamplifier and mixer of the ASR-8 were used without modification. Although the ASR-8 has a linear IF and in-phase and quadrature phase detectors, they were not used because a better receiver chain was available from a previous NAFEC project. WPL provided the range gate generator and buffer memory on a NOVA computer board. The computer and its peripherals were available from previous projects. The IMLAC graphics display proved unreliable and was replaced with a Tektronix graphics terminal. Software to observe the Doppler spectra at 8 range locations was developed. The Doppler spectra are calculated in software and are measured for only one range interval at a time. This was recognized as a limitation but it was deemed suitable for demonstration. [Equipment for calculating the spectra for 16 or more range intervals simultaneously is commercially available. Although the mean velocity could be calculated for all range intervals using the so-called pulse-pair technique, the complete Doppler spectra is needed for these tests where ground clutter is expected to be severe.] The software enables the operator to select the range delay to the first range interval, the spacing between intervals, the number of range locations (≤ 8), the number of spectra that would be averaged, and the scaling and baseline of the display. The number of points in the Doppler spectrum was fixed at 128. The unambiguous Doppler velocity is $\pm$ 27.55 m/s or about 0.43 m/s for each spectral point. The first tests of the system were made in June, 1978 when the radar-measured radial velocity profiles were compared with measurements made with an aircraft[10]. A second series of tests comparing radar and aircraft measurements has recently been made[11]. These tests demonstrate that the radial component of wind can be measured by Doppler radar in various types of weather. Not enough tests have been made to determine if measurements can be made in all weather regimes. However, measurements with a less sensitive radar[9] indicate that the NAFEC system should be able to measure radial wind profiles in the boundary layer practically all the time.

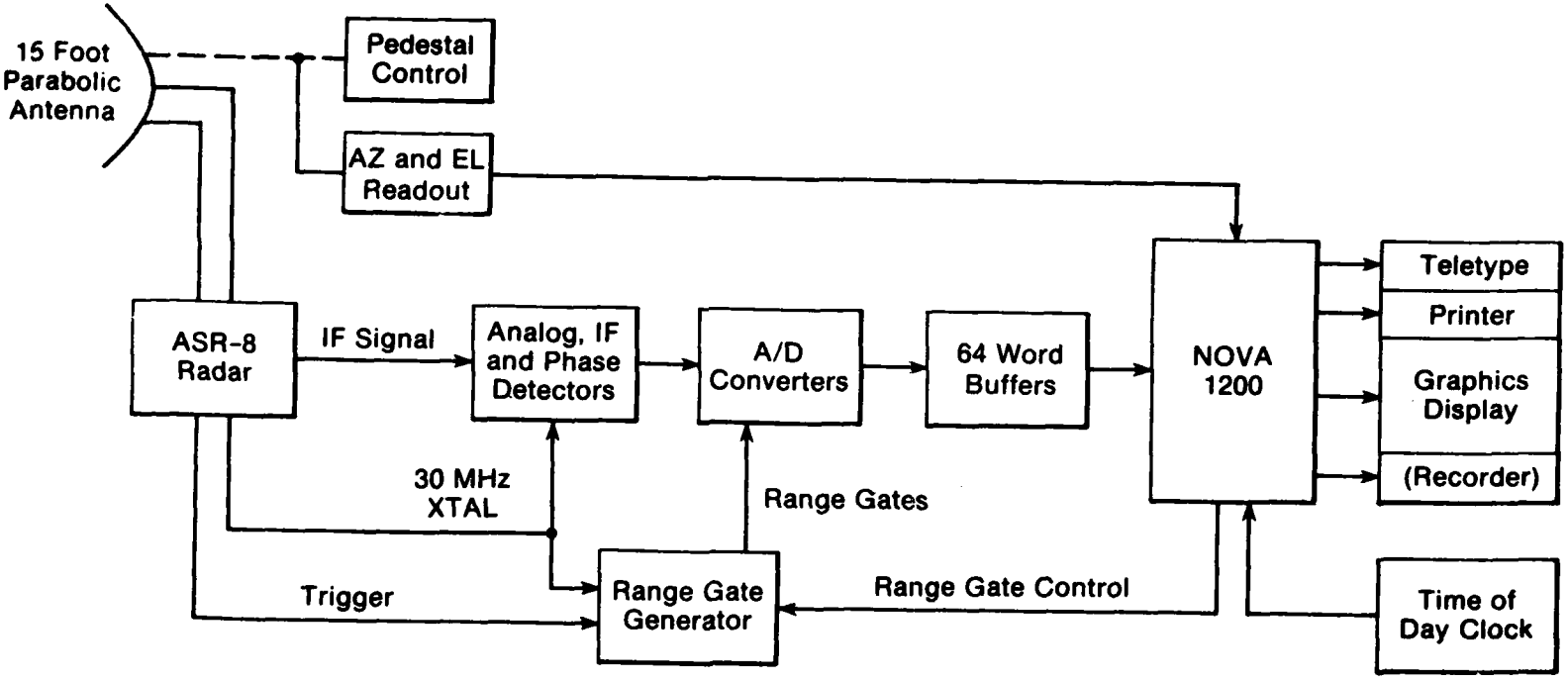

Figure 2.1. Block diagram of NAFEC wind shear detection system.

3. RADAR MEASUREMENT OF WIND PROFILES

If a radar is positioned at the end of a runway and is pointing along a 3 deg glide slope, it should be able to measure the headwinds encountered by the aircraft. (Headwind will be used to denote a headwind or tailwind; negative headwinds are tailwinds.) However, if there is vertical shear of this wind component, the radar will measure the actual profile only if its resolution is sufficient. For example, an antenna with a one-way beamwidth of 1.5 deg, (a value similar to that of the NAFEC test radar) would have a 2-way linear beamwidth of (0.018)R where R is the range. At a 3 deg elevation angle, the 2-way linear beamwidth is 0.342 h where h is the height. The actual wind profile will be filtered or smoothed by the radar resolution volume.

In phase 1 of this contract computer simulations were made to examine if a radar with a 1.5 degree beamwidth could resolve wind profiles used to represent hazards to low-level aircraft[12]. Figure 3.1 shows typical results. The actual wind, shown by solid lines, varies only with height. The expected value of the radar-measured wind profile is shown with diamond points. Note that the (unrealistic) gradients of the input profile are filtered by the vertical dimensions of the radar beamwidth. When the elevation angle is increased from 3 deg (a) to 6 deg (b), the vertical beamwidth at each measurement height is reduced by 2 so the radar resolution improves. The resolution continues to improve as elevation angle is increased until the vertical extent of the resolution along the beam becomes important. A pulse length of 1 microsecond (range resolution of 150 m) was used in the simulations. The radial resolution becomes more important than the cross-beam resolution for heights of 500 m or less when the elevation angle is greater than 14 deg. Therefore the ability of the radar to resolve low-level wind profiles will be best for elevation angles somewhat less than 14 deg.

The results from the simulations show that the radar can adequately resolve low-level wind profiles of the type that can be hazardous to aircraft. The Doppler radar can therefore serve the following functions:

a. measure vertical profiles of horizontal wind to 500 m altitude or more whenever the wind field varies only with altitude

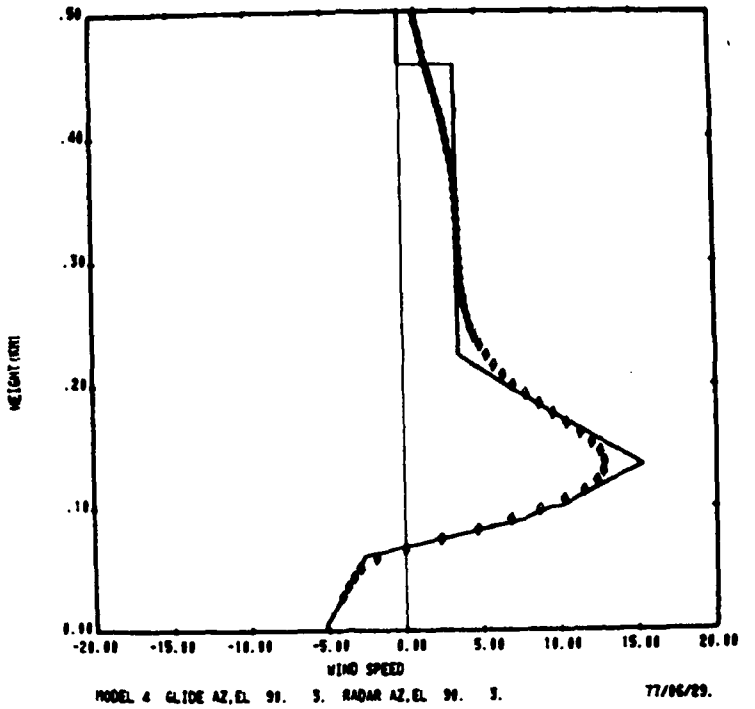

(a) Antenna elevation angle — 3 degrees.

Wind speeds are in meters per second.

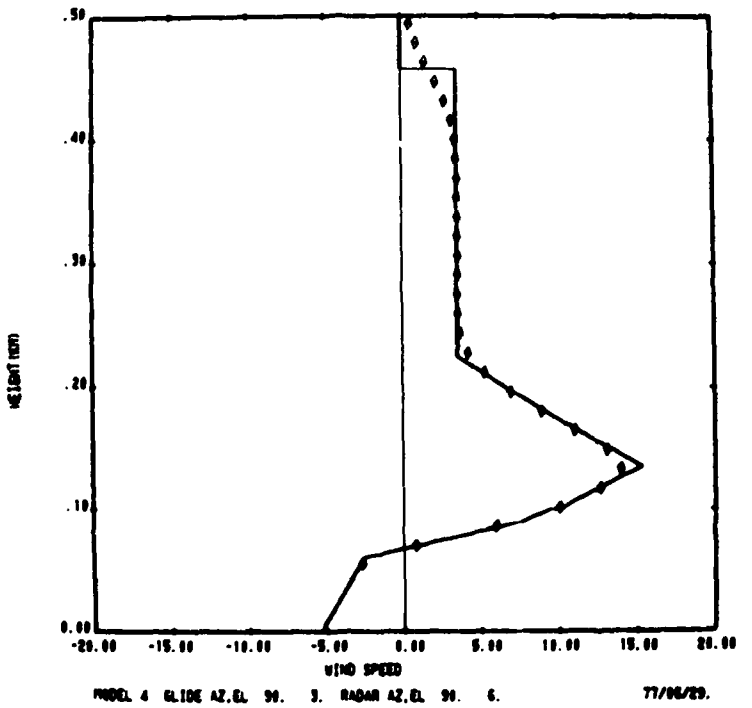

(b) Antenna elevation angle — 6 degrees.

Figure 3.1. Radar resolution of wind profiles.

b. measure vertical profiles of horizontal wind to 500 m altitude or more whenever the wind field varies with altitude and varies linearly with horizontal distance

c. measure the headwinds along approach and departure paths whenever the radar is located such that the aircraft track is approximately toward or away from the radar. The headwind component is more critical than the crosswind component for landing aircraft because changes in headwind cause air speed changes which cause approaches to be long or short

d. if the radar is not suitably located for measuring headwinds along the aircraft track, the radar can measure the radial velocity profile along the approach path and check to see if it is consistent with the vertical profile of horizontal wind.

A single Doppler radar can measure vertical profiles of horizontal winds for uniform or linear conditions; however, the profile measured at the radar site is not applicable to the aircraft track located some distance away if there are horizontal gradients. If the horizontal wind field varies only with height, then the radar-measured wind profile can be directly applied to landing aircraft. Therefore, the radar can be used to measure wind profiles as in (a) and (b) and to check the applicability of the measured profile as in (c) or (d).

The most widely used method of measuring wind profiles with Doppler radar is the velocity-azimuth display (VAD) method[13]. The radial velocity is measured at each height as a function of azimuth (continuously or discretely) with a fixed antenna elevation angle. Fourier analysis[14] of the radial velocity measurements gives not only the mean wind, but also the shearing and stretching deformations, $(\frac{\partial u}{\partial y} + \frac{\partial v}{\partial x})$ and $(\frac{\partial u}{\partial x} - \frac{\partial v}{\partial y})$, and the vertical motion and/or divergence $(\frac{\partial u}{\partial x} + \frac{\partial v}{\partial y})$. Here, u, v, w are the wind components, which will be averages over a circle of radius $z/\tan\theta_E$ where z is the measurement height and θ_E is the antenna elevation angle.

A simplified version of the VAD scan, used in the Dulles wind shear system[4], is useful for measuring mean wind profiles routinely. This method involves measuring the radial velocity profile at 4 azimuths separated by 90 deg. This method

allows the use of fixed antennas which may be less costly than a single antenna and pedestal. Let the [u, v] wind components be defined by the orthogonal pointing directions. Then the 4 radial velocity measurements are:

$$V_1(h) = u_1(h)\cos\theta_E + (w + V_t)_1(h)\sin\theta_E$$
$$V_2(h) = v_2(h)\cos\theta_E + (w + V_t)_2(h)\sin\theta_E$$
$$V_3(h) = -u_3(h)\cos\theta_E + (w + V_t)_3(h)\sin\theta_E$$
$$V_4(h) = -v_4(h)\cos\theta_E + (w + V_t)_4(h)\sin\theta_E.$$

V_t is the fall speed of the scatterers when there is no vertical wind. V_t is zero for refractive turbulence scattering but can be as large as 9 m/s in precipitation[15] and even larger if there are hail particles.

If the vertical motion is assumed to be the same at the 4 measurement points (or if the elevation angle is low), then the u and v profiles are found from:

$$u(h) = \frac{u_1(h) + u_3(h)}{2} = \frac{V_1(h) - V_3(h)}{2\cos\theta_E}$$
$$v(h) = \frac{v_2(h) + v_4(h)}{2} = \frac{V_2(h) - V_4(h)}{2\cos\theta_E} .$$

Thus under this assumption the wind profile is measured correctly for a uniform horizontal wind or a horizontal wind that varies linearly with distance. The error in u or v caused by changes in vertical motion between opposite measurement points is $[\Delta(w + V_t)][\tan\theta_E]$ or $(h)[\text{gradient}(w + V_t)]$. The vertical motion cannot be found unless the horizontal wind field is uniform. Just as in the complete VAD analysis technique, the vertical motions cannot be separated from gradients of horizontal wind. This simplified method of wind profile measurement is preferred to the full VAD technique for precipitation-free conditions because of the long dwell times needed at each azimuth. The largest error of horizontal wind caused by the fall speed of raindrops occurs if the scattering in one direction is from refractive turbulence or very small raindrops with near-zero fall speed and the scattering in the opposite direction is from large raindrops. The maximum error would be $9\tan\theta_E$ or less than 2 m/s for elevation angles as high as 12 deg. Note

the sum of the radial velocity measurements made in opposite directions will be a measure of vertical particle velocity and horizontal wind gradient. That is:

$$V_1(h) + V_3(h) = [u_1(h) - u_3(h)] \cos\theta_E + [(w + V_t)_1 + (w + V_t)_3] \sin\theta_E .$$

Since the contributions to this sum from the fall speed of raindrops and normal vertical air motions are bounded, this sum should not deviate from zero by more than a few m/s. If it does it is an indication of extreme vertical motions such as from hailstones or strong vertical drafts or an indication of horizontal wind gradients. The sum of the radial measurements is one check of whether the measured profile is applicable to points other than a line above the radar. Additional tests of whether the measured profile is representative of the wind some distance away from the radar can be made by measuring the wind profile at different elevation angles and different azimuth angles.

Another check of whether the radar-measured wind profile is valid along the aircraft track can be made by measuring the radial velocity along the track, and comparing the measurements with the expected value. That is, the measured velocity along the aircraft track is $u \cos\beta \cos\theta_E + v \sin\beta \cos\theta_E + (w + V_t) \sin\theta_E$. The measurement must be consistent with the radial velocity predicted with this equation with u, v, and $(w + V_t) \sin\theta_E$ found from the 4-point profile measurement.

The conclusions from phase 1 simulations were that radar wind profiles could be measured by Doppler radar and that a radar located near the intersection of major runways could measure the profile of headwind along approach and departure paths. In general, however, a single radar is not able to measure winds along the approach or departure path of all runways and wind profiles measured at the radar cannot be applied to the aircraft track in the case of hazardous winds from localized, transient phenomena.

4. RADAR DETECTION OF WIND SHEAR

A Doppler radar can measure only the radial component of the wind so it cannot, in general, measure the horizontal winds along the aircraft track. If one radar is to provide wind shear warning data for the entire airport it must be able to detect hazardous winds regardless of its location relative to any one approach path. Transient events, such as gust fronts or outflow from thunderstorms produce locally complex wind fields that cannot be directly measured with a single Doppler device.

Complex three-dimensional wind fields can be measured with suitably placed multiple Doppler radars. However, the data processing used to achieve these wind fields is performed off-line and multiple Doppler systems are generally viewed as research devices. One of the research outputs of multiple Doppler experiments (one that has been largely ignored) is to determine what information about the complex dynamics of atmospheric motion could be derived from a single Doppler radar. When (single) Doppler radars become operational tools, as expected in the next generation of weather radars, there should be increased emphasis on deriving maximum utility from single radar. While a complete dual-Doppler radar system which derives horizontal wind fields in real time could be constructed, (using two radars located 10-20 km from the airport such that 2-dimensional data for all approach and departure paths would be obtained) such a system would be complex and would have relatively poor altitude resolution unless the antenna apertures were very large. A possible solution for the wind shear problem would be to locate radars near the intersection of major runways so that the headwind component could always be observed. The radars could use a common data system so only the transmit/receive units and the antennas would need to be at the runways. If these runway radars were required to operate only during precipitation, then low power and inexpensive radars (X-band with a 1 m diameter antenna) for each runway could be a practical solution. These radars would complement a single scanning radar that could measure wind profiles in all-weather. If the runway radars were required to measure winds in all weather situations, the FM-CW radar may provide a practical solution[9]. In this case, the runway radars would complement

a single scanning Doppler radar that would not have to measure wind profiles in all-weather. Rather, it could be a NEXRAD[6] radar, located some distance from the airport, and used primarily for storm surveillance.

Efforts have been made to use data from a single radar to obtain two dimensional wind fields. One method, tested on a convective storm, measured the motion of the reflectivity patterns by correlating reflectivity fields measured about 2 minutes apart[16]. The motion of fine scale patterns in the radial velocity field can also be measured by correlation of radial velocity fields measured at different times[17]. Experiments in the optically clear air show that these eddy fields remain correlated so that their motion can be measured. The spatial resolution for winds derived from correlation methods will be much poorer than for dual Doppler measurements because relatively large sections of data must be used to obtain the motion of a feature or perturbation of the radial velocity field or reflectivity field. Other methods of obtaining wind fields from single Doppler radar involve combining data obtained from a sector scan[18] or volume scan[19]. Since these methods also use data from many radar resolution volumes to derive wind field data, the resolution will be relatively poor and not suitable for low-level wind shear detection.

If a single radar measures the radial velocity at 2 points near the glide slope, then a 2-dimensional wind vector can be calculated if vertical motion is neglected. A radar located relative to the runway approach path as in Fig. 4.1 cannot directly measure the headwind component encountered by the aircraft. However, by measuring the radial velocity at A and B, the longitudinal velocity (V_L) and transverse velocity (V_T) can be derived at P so that both headwind and crosswind can be found on the aircraft approach path. At first glance this appears to be a method which does not rely on assuming a uniform wind over a large distance, but with further analysis it is seen that the method fails if there are wind gradients. First, assume that the winds are locally constant; that is, the wind is the same at A, P, and B. Let the antenna elevation angle be zero to simplify the equations. The transverse velocity at P is given by

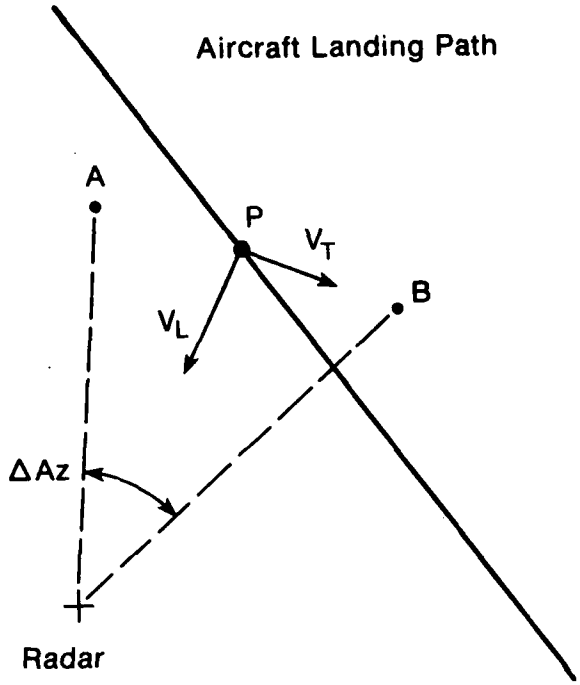

Figure 4.1. Single Doppler radar measurement of two-dimensional winds.

$$V_T = \frac{V_A - V_B}{2 \sin(\frac{\Delta AZ}{2})}$$

where V_A and V_B are the radar-measured radial velocities at A and B. The longitudinal velocity at P is given by

$$V_L = \frac{V_A + V_B}{2 \cos(\frac{\Delta AZ}{2})}$$

or it can be measured directly at P by the radar. The uncertainty in measurement of V_T is given by

$$\Delta V_T = \frac{\Delta V_R}{\sqrt{2} \sin(\frac{\Delta AZ}{2})}$$

where ΔV_R is the uncertainty in the measurement of radial velocity which is assumed to be the same at A and B. Thus, if the radial velocities are measured

with an uncertainty of 0.5 m/s, the transverse velocity is measured with an uncertainty of 2 m/s for $\Delta AZ = 20$ deg. If ΔAZ is smaller, then the assumption of locally constant wind is made for a smaller area, but the error in transverse velocity increases for a given measurement accuracy.

However, suppose there are wind gradients and the two-point method is used because it is believed that if the measurements are made at closely separated points then the locally constant assumption would still be valid. The transverse velocity is given by

$$V_T = \frac{V_A - V_B}{2 \sin(\frac{\Delta AZ}{2})} + 2 \overline{k_{LT}} R \cos(\frac{\Delta AZ}{2})$$

where R is the distance from the radar to P and $\overline{k_{LT}}$ is the average change in V_L per unit transverse distance. In the limit of small angles,

$$V_T = \frac{V_A - V_B}{\Delta AZ} + 2 \overline{k_{LT}} R$$

so that no matter how small the measurement separation the gradient term introduces errors. Decreasing the separation angle not only increases the measurement uncertainty (first term) but also increases the errors caused by gradients. R is of the order 10^3 to 10^4 m and $\overline{k_{LT}}$ is 10^{-2} to 10^{-3} s^{-1} in dangerous shear so the errors are too large for useful measurements whenever there are dangerous wind shears. Thus, a single Doppler radar cannot adequately measure the winds encountered by the aircraft in those cases where complex 3-dimensional wind fields are expected.

Even if a single-Doppler radar cannot measure the wind profile along the aircraft track, it may be able to detect dangerous winds from radial velocity measurements. The <u>profile</u> of radial wind along the aircraft track and the <u>field</u> of radial velocity measurements in the space near the track may be sufficient to detect dangerous winds. Radar measurements provide V_r and its gradients $(\frac{\partial V_r}{\partial r}, \frac{\partial V_r}{\partial \theta_E}, \frac{\partial V_r}{\partial Az})$. If the radial velocity fields measured by a scanning Doppler radar are displayed in color on a PPI indicator, characteristic features of

certain types of velocity fields are readily identified[20]. Contours of constant radial velocity are radial lines (Fig. 4.2) if the wind field is uniform. Non-uniform wind fields cause a distortion of these contours. The color displays showing mesocyclone circulation in tornadic storms[6] are the best example of the detection of hazardous winds by single Doppler radar. Another display technique that has proven useful for single Doppler radar data is the multi-moment vector display[21]. Features such as outflow from symmetrical downdrafts or "downbursts" should be easily detected in the pattern of the radial velocity field[12]. If a single Doppler radar is to provide a wind shear warning system for an entire airport runway complex (where it cannot point along all

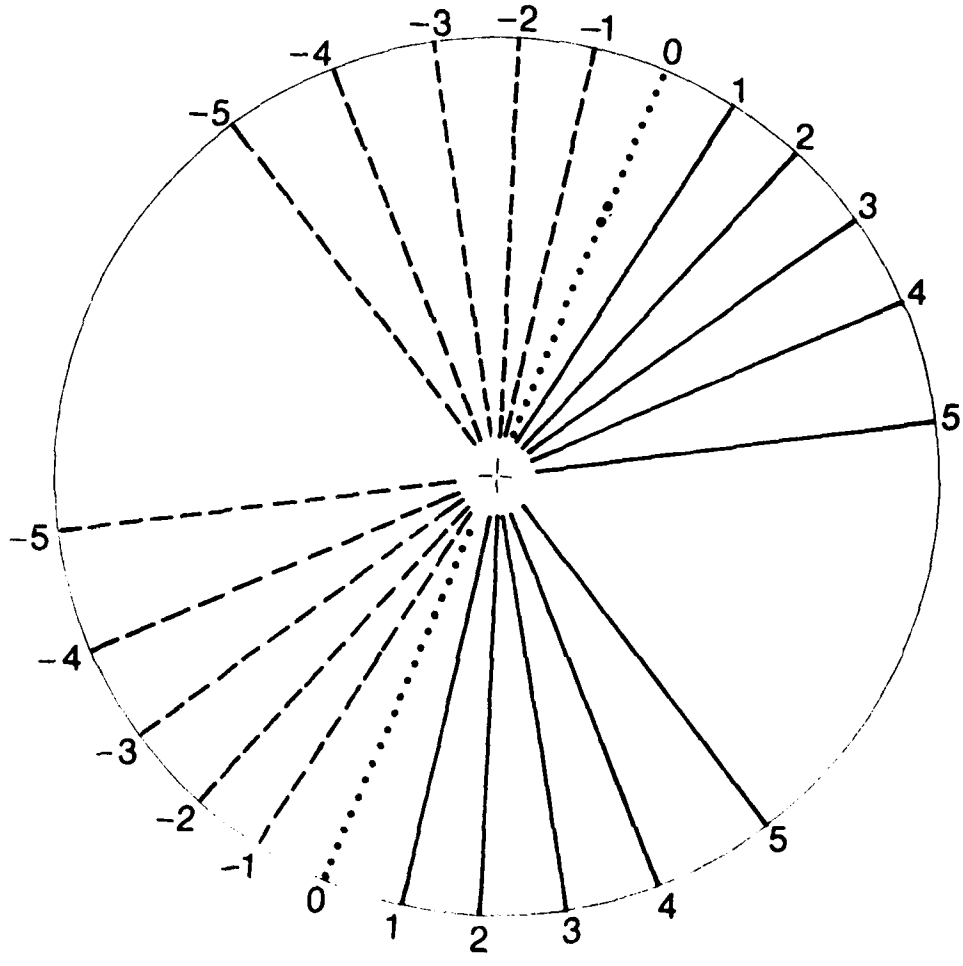

Figure 4.2. Contours of constant radial velocity for a uniform wind field as they would appear on a PPI.

runway and departure paths), then it must be able to detect dangerous wind gradients in the radial velocity field. A computer simulation study has been made to determine if the radar-measured radial velocity could detect wind shear in wind field models used to simulate low-level wind shear hazards.

5. SIMULATION PROGRAM

The computer program used in phase 1 simulations[12] was expanded to calculate and display the actual crosswind and vertical wind (in addition to the headwind) encountered by the aircraft on the approach path. The expected value of the radar-measured radial velocity is also calculated and displayed. In phase 1 simulations the radar-measured radial velocity was calculated by integrating the actual point radial velocity function over the entire radar resolution volume. The purpose of this integration was to test if the radar could resolve the existing wind profile. Although the integration remains part of the simulation program, it was generally not used for these tests. Rather, the radar-measured radial velocity was usually taken as the point value at beam center. Phase 1 simulations showed that realistic low-level profiles could be resolved; these simulations are intended to determine if wind shear can be detected in the radial velocity field.

Figure 5.1 shows the geometry for the simulation program. (The setup is similar to that used for phase 1 simulations. In the present case the location and orientations of the runway are also variable.) Radar range, azimuth, and elevation (R, AZ, EL) are related to the (x, y, z) coordinates as follows:

$$x = R \sin AZ \cos EL + X_R$$

$$y = R \cos AZ \cos EL + Y_R$$

$$z = R \sin EL + Z_R$$

where (X_R, Y_R, Z_R) are the coordinates of the radar location. The aircraft position (X_G, Y_G, Z_G) is given by:

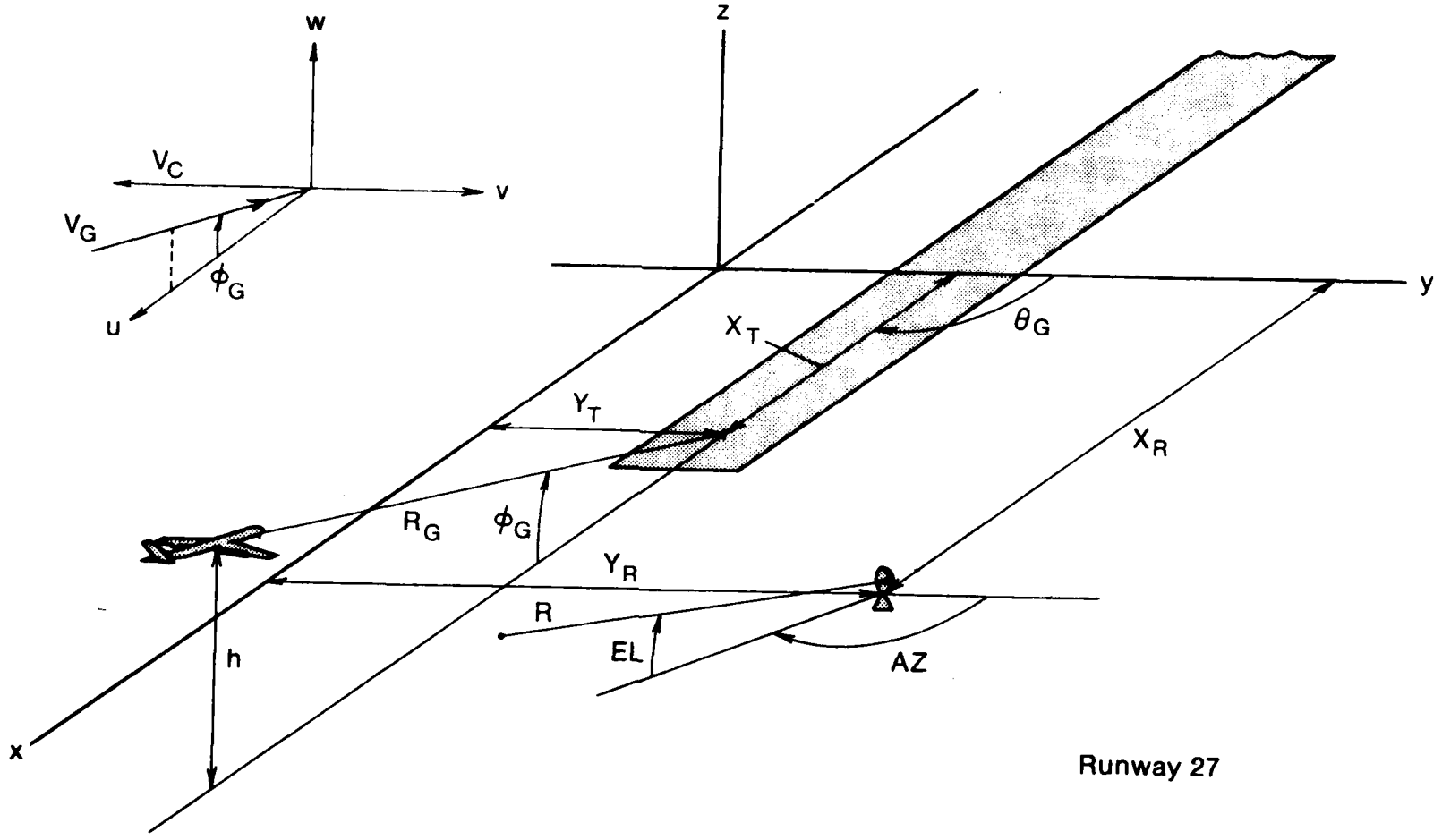

Figure 5.1. Coordinate system for the simulation program.

$$X_G = R_G \cos\phi_G \sin\theta_G + X_T$$

$$Y_G = R_G \cos\phi_G \cos\theta_G + Y_T$$

$$h = Z_G = R_G \sin\phi_G + Z_T$$

where (X_T, Y_T, Z_T) are the coordinates of the touchdown point, R_G is the distance from the aircraft to touchdown, ϕ_G is the glide slope angle, θ_G is the runway orientation, and h is the height of the aircraft. The runway orientation, θ_G, is (10 x runway number - 180) deg. The program allows for arbitrary location of both the radar and the runway relative to a (u, v, w) wind field model that is referenced to the origin. In all the simulations the glide slope angle was 3 deg, and (X_R, Y_R, Z_R) and Z_T were taken as zero.

The headwind, crosswind, and vertical wind encountered by the radar (V_G, V_c, W) are:

$$V_G = u_G \sin\theta_G \cos\phi_G + v_G \cos\theta_G \cos\phi_G + w_G \sin\phi_G$$

$$V_c = v_G \sin\theta_G - u_G \cos\theta_G$$

$$W = w_G,$$

where, in this notation u_G, v_G, w_G are the u, v, w wind components on the glide slope; i.e., $u_G = u(X_G, Y_G, Z_G)$ etc.

The position of the aircraft in radar coordinates is

$$R_A = [(X_G - X_R)^2 + (Y_G - Y_R)^2 + (Z_G - Z_R)^2]^{1/2}$$

$$A = \tan^{-1}\left[\frac{X_G - X_R}{Y_G - Y_R}\right]$$

$$E = \sin^{-1}\left[\frac{Z_G - Z_R}{R_A}\right] .$$

The radial wind component, that component observed by the radar, is

$$V_R = u \sin AZ \cos EL + v \cos AZ \cos EL + w \sin EL ,$$

where (u, v, w) are the wind components at (R, AZ, EL). In particular, along the glide slope, the radial velocity is

$$u_G \sin A \cos E + v_G \cos A \sin E + w_G \sin E.$$

The input wind models are in Cartesian coordinates and the wind components and radial wind at any point are calculated using the above equations.

One of the computer outputs is a plot of the actual wind (V_G, V_c, W) and the radial wind component along the glide slope. The simulation program also calculates the radial velocity field as would be observed by a scanning Doppler radar. In all cases, the radar-measured velocity was taken as the radial velocity at beam center to avoid excessive calculation time. Two types of scans were programmed: a volume scan and a constant elevation scan. The volume scan was centered at the point where the aircraft position is 250 m above touchdown. The scan covers an azimuth and elevation sector to scan the entire glide path for h = 0 to 500 m and covers 12 km in range. The azimuth sector size depends on the radar location and is typically 60 deg. The computer selects the required azimuth sector (from 40 to 180 deg in 20 deg increments). The elevation scans extend to the elevation angle required to intersect the 500 m height of the glide slope. The scan increments are 0.1 deg in elevation, 300 m in range, and the azimuth sector is covered with 40 increments. The output can be displayed as: (a) contours of constant radial velocity as a function of azimuth and the height that the scan intersects the glide slope, or (b) contours of constant radial velocity as a function of range and the intersection height. Small arrows on these plots indicate where the glide slope intersects the data surface.

The constant elevation scan is also centered at the point where the aircraft position is 250 m above touchdown. Here, the scan intersects the glide slope at only 1 point. The output is displayed as contours of constant radial velocity as a function of range and azimuth.

Realistic runway configurations and radar locations such as shown in Fig. 5.2 (representing O'Hare International Airport) were used. Runways 14R, 4R and 9L were used as representative of approach paths relative to the ASR-8 location. The simulation program is described in Appendix I.

6. WIND MODELS

Wind models available in the computer simulation program include both analytic and numerical models of 1, 2, and 3 dimensional wind fields. Models 1-6 are the same models used in phase 1 simulations.

Models 1-3 are 1-dimensional models or vertical profiles of the horizontal wind. The vertical wind is zero. These models were developed by Fichtl and Camp[22]. Model 1 is a logarithmic profile representing the wind in the neutral boundary layer. Model 2 represents frontal winds and model 3 represents the nighttime stable boundary layer.

Model 4 (also from Fichtl and Camp) represents the wind profile of cold air outflow from a thunderstorm along the glide slope. It includes vertical winds but it is not a thunderstorm model; it represents the winds along a line through a storm. Model 5[23] is a vertical profile of horizontal wind that is constant in direction and with no vertical wind. It was found to be difficult for pilots to handle in flight trainers. Model 6 is a 3-dimensional analytic model of an axially symmetric downburst from a thunderstorm. The center of the downburst (X_c, Y_c) can be positioned at any point relative to the origin.

Models 7-12 are variations of model 6. Model 12 has the same functional form as model 6 but with different scale height and wind speed. Model 7 is the sum of models 1 and 12. Models 8-11 are model 12 with constants added to the u and v components, i.e., an axially symmetric downburst with translation. The downburst is translated by u = 10 m/s in model 8, u = 20 m/s in model 9, v = 10 m/s in model 10 and v = 20 m/s in model 11. (The translation is constant with height above 10 m altitude and below 10 m it decreases linearly to zero at the surface.

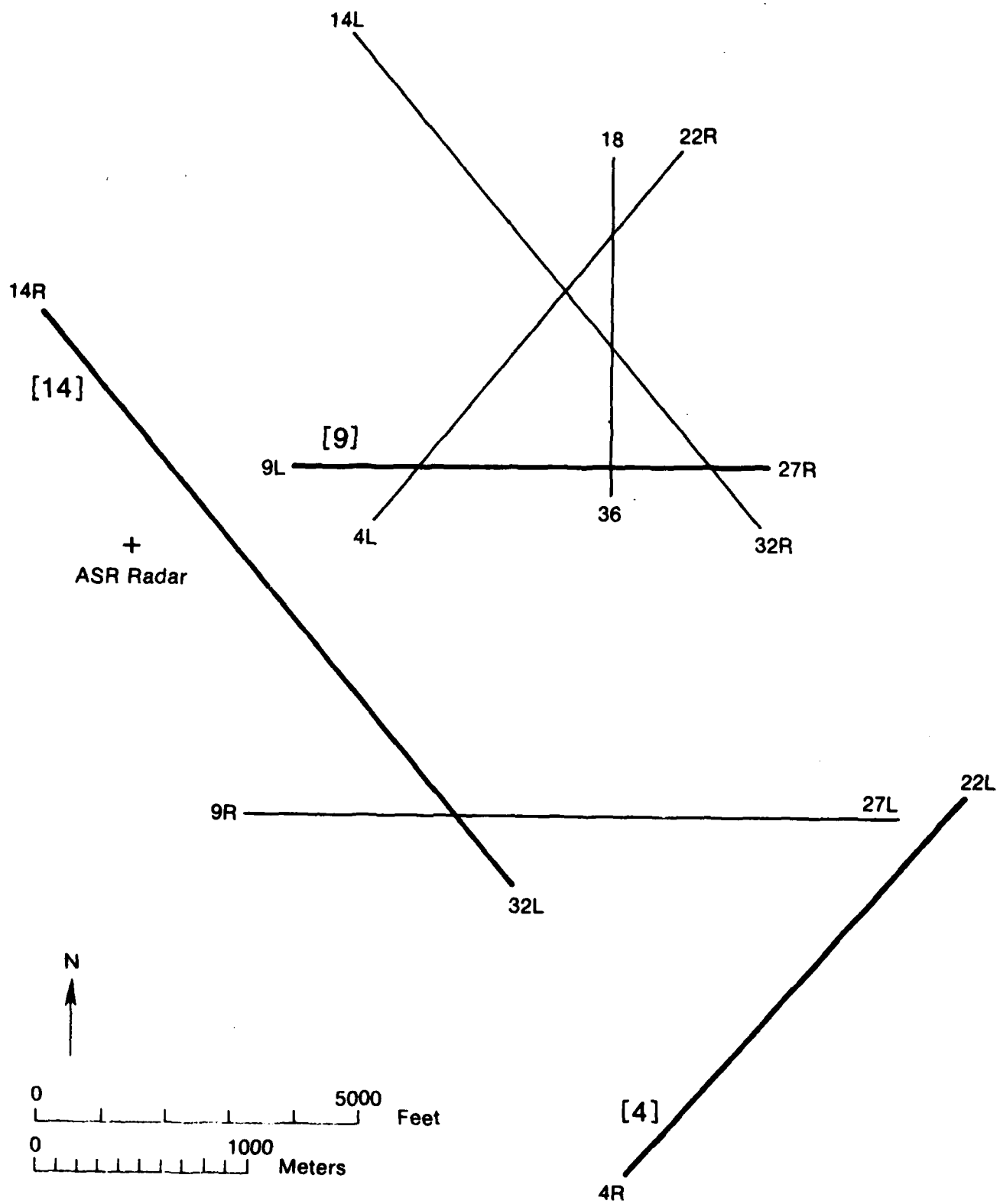

Figure 5.2. Runway layout (similar to O'Hare International Airport) used in the simulations.

Models 21-25 are "shear-line" models; an abrupt wind shift occurs along a line. In models 21-24 the winds on one side of the line are toward the line at 25 m/s on one side and away from the line at a 45 deg angle at 5 m/s on the other side. In model 21 the line is oriented north-south the winds toward the east and NE. In model 22 the line is NE-SW with the winds toward the SE and E. For model 23 the line is E-W with the winds toward the S and SE. For model 24 the line is N-S with the winds toward the W and SW. Model 25 is the same as model 21 but with an altitude weighting function that is zero at the surface, increases to unity at 100 m altitude and decays asymptotically to zero above 100 m altitude.

Models 41-50 are numerical models used by the FAA in studies of wind-shear conditions that were related to aircraft incidents. They were furnished to WPL by H. Schlickenmaier (ARD-731). These models are expressed in a Cartesian coordinate system centered at the touchdown point, $(X_T, Y_T, 0)$. The winds in the Cartesian coordinate system defined in section 5 are found by coordinate transformation and linear interpolation is used to obtain values needed at points scanned by the radar.

Models 41, 42, 43, and 45 are one-dimensional models — vertical profiles of horizontal wind with no vertical velocity. Model 41 is a logarithmic profile that represents the neutral boundary layer. Models 42 and 45 are frontal wind models related to incidents at Tokyo and Boston. Model 43 is from a profile along the glide path in a thunderstorm.

The other models are two-dimensional wind fields which represent the horizontal and vertical winds in a vertical plane through the approach path. Models 44, 46, 47, 48 and 50 represent thunderstorm winds and model 49 is for a frontal wind. The data are supplied as vertical wind profile at various horizontal distances from touchdown.

For models 1-5 and 21-25 the wind speed and direction are the same for all simulations and the viewing direction of the radar is varied by selecting different runways. This shows how the radial component of the same wind profile would appear with different observation angles. For models 6-12, the location of the downburst, and therefore the wind speed and direction, are varied depending on the runway. For models 41-50, the wind input is relative to the touchdown

point so the wind field relative to the fixed coordinate system and the radar scanning direction depends on the runway selected.

The sign convention used is that positive radial wind is away from the radar, positive glide slope wind is a headwind for a landing aircraft, positive crosswind causes a landing aircraft to drift right and positive vertical wind is upward.

7. SIMULATION RESULTS

A large number of simulation runs were made (27 wind models X3 runways) with 5 or more output plots for each case. Samples of various configurations are included in this report. Other output plots are available on microfilm. Outputs with other wind models and runways could be simulated with the flexible computer program that has been developed. Wind speeds shown in figures 6.1 through 6.21 are in meters per second.

A. Radial Velocity Profiles (Figures 6.1-6.21)

Model 1, a logarithmic one-dimensional profile, has constant wind direction from the west and wind speed that increases to 30 m/s at 500 m altitude. This is the actual headwind that would be encountered by a landing aircraft to Runway 9, ([9]). Figure 6.1 shows the glide slope headwind as a solid line and the radar-measured radial velocity along the glide slope as diamond points. The crosswind (shown as a dashed line) and the vertical wind (shown as a dotted line) are both zero for this model. The radial velocity changes from toward the radar to away from the radar as the azimuth angle passes due north in a clockwise scan. Note that the radar viewing angle becomes normal to the approach path for runways 9L, 9R, 4L, and 36 (Fig. 5.2). For these runways the sign convention could be changed so that the radar-measured radial velocity would be positive for velocities toward the radar whenever the viewing direction was toward the runway. If this were implemented for Fig. 6.1, all the diamond points would indicate negative radar-measured radial velocity, with a zero at the point where the radar viewing angle was normal to the approach path. However, if there is crosswind, the radial

velocity may become zero at any azimuth angle or it may never be zero depending on the magnitude and direction of the crosswind. Changing the sign convention would then introduce a discontinuity in the profile, so this was not implemented. The identification at the bottom of each figure shows the wind model, the runway, the coordinates of the touchdown point and the coordinates of the radar. The storm location for models 6-12 is the location of the center of a downburst. The last identifier shows whether the radar measurements were derived by integrating over the pulse volume (INTT) or if the value at the center of the pulse volume was used (INTF). Figures 6.2 and 6.3 show how the same wind is encountered by aircraft and observed by radar along the approaches to [4] and [14]. Crosswind and headwind are present on both paths. A radar at the end of the runway would measure the solid line in each figure. If the radar had also been used to measure wind profiles as discussed in section 3, the diamond points could be predicted from the profile measurements. In addition, for this wind model and all other one-dimensional models the radar would have measured the glide slope wind (the solid line) for each runway if the radar antenna had been pointed parallel to the approach path. The radial velocity measurements along the glide slope may not show as abrupt a change with altitude as the wind components (see Fig. 6.2) because of the viewing angle. Note also that if the wind field had been constant in speed and direction with altitude, the radar-measured radial velocity would still show a change with height. Thus the rapid change from negative to positive velocity at low altitude in Fig. 6.1 is primarily a result of change in observing direction. The radial profile, by itself, is not easily interpreted. Wind models 3 and 5 are also one-dimensional with constant wind direction. Radial velocity profiles along the glide slope are basically the same as those in Fig. 6.1-6.3.

Wind model 2 is a one-dimensional profile that includes wind direction change with altitude. Wind is from the west at the surface but changes to northwest starting at 30 m altitude. Figure 6.4 shows the profile along the approach to [9]. The radial velocity is determined primarily by the tail wind below about 30 m altitude and above about 100 m altitude. From 30-100 m the radial velocity depends mainly on the crosswind. A radial profile of this type would be indicative of shear rather than just the change in viewing direction because the changes in slope of the radar-measured profile indicates that it is not a portion of a sinusoid as it would be for uniform winds. Below about 100 m altitude the crosswind component becomes significant in the radar measurement.

Wind model 4, a one-dimensional representation of cold air outflow from a thunderstorm, includes vertical winds. The glide slope profiles for all 3 runways (Figs. 6.5-6.7) are very different but each is clearly indicative of shear along the path.

Figure 6.8 is representative of the glide slope profiles of the downburst model (models 6 and 12). In simulations with these models, the downburst is always positioned near the approach path of the runway that is being scanned. The profiles are similar for all runways because of the axial symmetry of the wind model. The profile depends on the location of the runway and downburst relative to the radar location.

Figure 6.9 shows how the glide slope profiles change when the downburst model is translated with a 20 m/s wind from the west. The radial velocity pattern of the downburst (Fig. 6.8) is translated by a portion of a sinusoid. In Fig. 6.10 the translation of the radial velocity profile on [9] includes that portion of the sinusoid which is changing rapidly (below 50 m altitude) so the actual velocity profile is altered significantly. If the translation can be measured and its effect removed from the radial profile, then the basic features of the downburst model are observed.

Figure 6.11 illustrates the simulation results with wind models with an abrupt wind shift along a line. The gradual change in radial velocity at upper altitudes is caused by the change in viewing direction. The velocity changes slowly with altitude as compared to [9], because the range to [4] is greater so smaller azimuth angles are used to scan the 0-500 m height interval. The abrupt change in radial velocity would not be observed if the filtering effect of the radar resolution volume had been incorporated in the simulation.

For models 41-50 the input wind field is expressed relative to the runway. Therefore the actual wind profiles along the glide slope are the same for all runways. The wind fields are one- or two-dimensional (no variation in wind in the horizontal direction normal to the approach path). Simulations using these models show how the same wind encountered by the aircraft appears as a different radial velocity profile for different viewing directions whereas simulations with models 1-25 show how the same wind throughout the airport appears for various viewing

directions. Figures 6.12-6.14 illustrate the simulation results for model 42, a one-dimensional frontal wind. These figures and Fig. 6.1-6.3 illustrate the differences in the input wind models described above. Note in Fig. 6.12 that the crosswind is so large that the measured radial velocity is determined primarily by crosswind. The same wind model, when observed on runway [9], shows crosswind at low altitudes but not at higher altitudes.

Figure 6.15-6.17 show the profiles along [4], [9], and [14] for model 49, a two-dimensional frontal wind model. This is a numerical model with relatively coarse resolution and the linear interpolation required to transform the input data to wind components at any point makes the actual profile appear as line segments rather than smooth curves. The radial velocity profiles are similar for all 3 runways because of the similarity in the structure of the headwind and crosswind.

Model 50 is a two dimensional numerical model representing outflow from a thunderstorm that was associated with a June 24, 1975 accident at John F. Kennedy International Airport. Large vertical velocities are included but they will not be observed by Doppler radar at low elevation angles. The velocity profiles are very similar to some of the downburst profiles obtained with the analytical model with translation. The radial velocity profile shows the strong gradients of tailwind.

Comparison of the headwind profiles and the radar-measured radial velocity profiles shows that, for the wind models used in these simulations, the radar can adequately measure the headwind (within 2 m/s) even if there is some offset of the radar from the runway. The radar measurements can be taken as headwinds along the approach to [14] and the portion of the approach to [9] that is above about 100 m altitude. Measurements along the approach to [4] are strongly influenced by crosswinds. It can be seen from Fig. 5.2 that headwinds along the approaches to 14R, 32L, 22R, and 27R could be measured by the radar, and headwinds could be measured along the approaches to 27L, 9L, 9R and 4L for that portion of the path that is above 100-200 m.

In addition to the profiles of radial velocity and glide slope winds as a function of height, the simulation program also outputs the profiles as a function of distance from touchdown. Figure 6.21 is a sample of this output; the profiles are the same as those shown in Fig. 6.10.

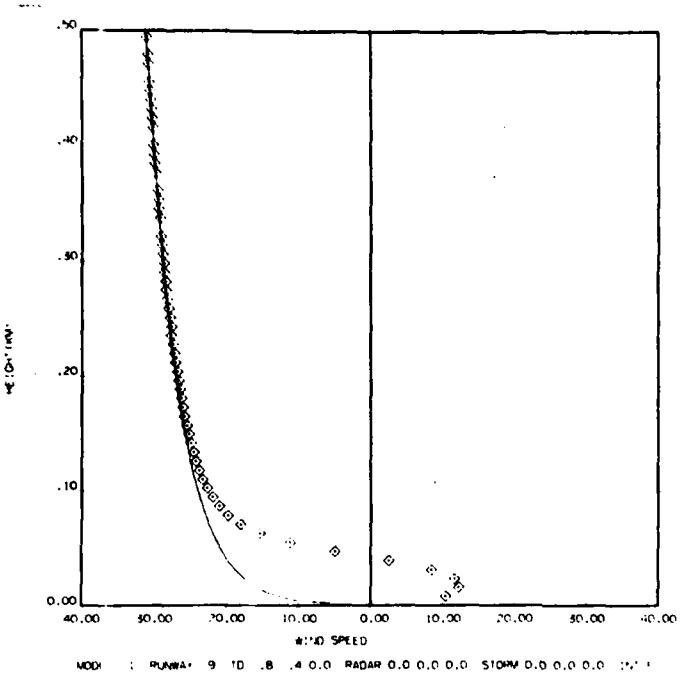

Figure 6.1.

WIND SPEED-HEIGHT PROFILES

Solid lines show headwinds (+) or tailwinds (-) encountered by a landing aircraft at various heights above touchdown. Dashed lines show crosswinds and dotted lines show vertical winds along the approach path. Positive crosswind causes a landing aircraft to drift to the right and positive vertical wind is upward. Diamond points are the expected value of radar-measured radial velocity as the radar scans along the approach path. Positive radial velocity is away from the radar.

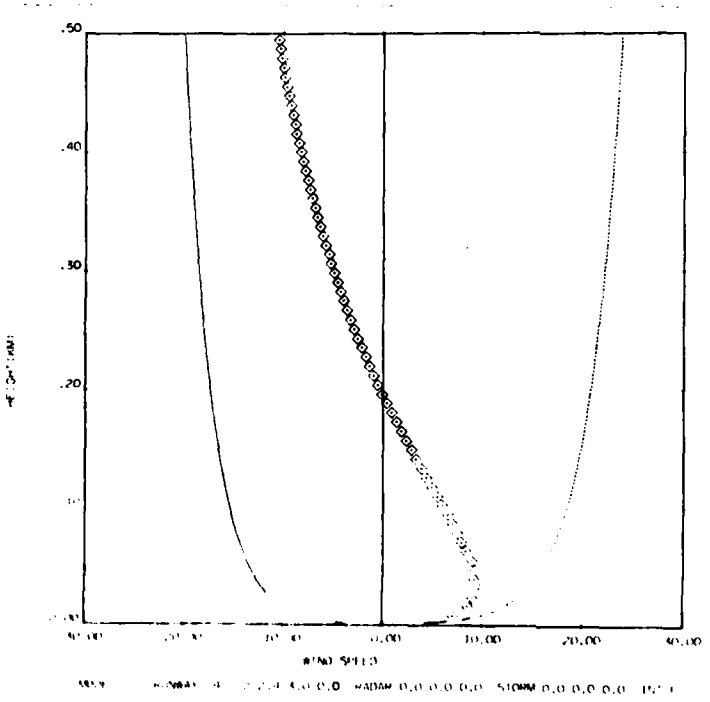

Figure 6.2.

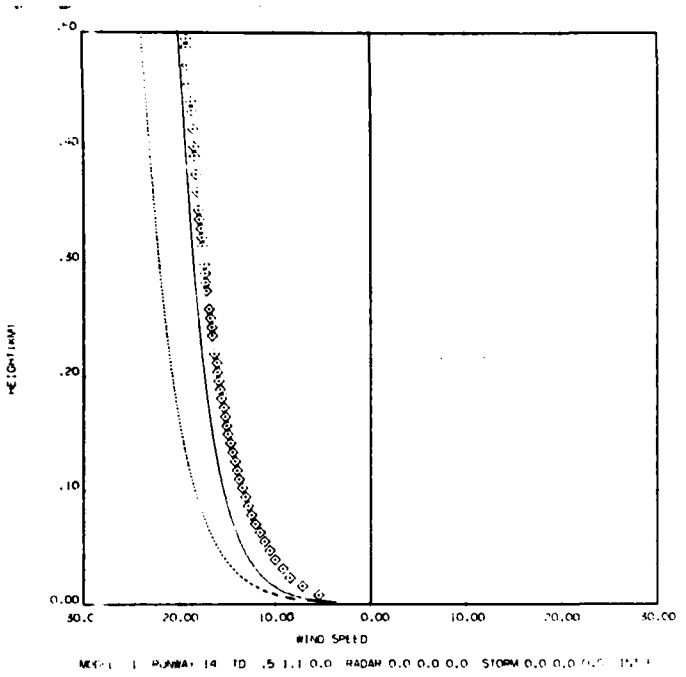

Figure 6.3.

WIND SPEED-HEIGHT PROFILES

Solid lines show headwinds (+) or tailwinds (-) encountered by a landing aircraft at various heights above touchdown. Dashed lines show crosswinds and dotted lines show vertical winds along the approach path. Positive crosswind causes a landing aircraft to drift to the right and positive vertical wind is upward. Diamond points are the expected value of radar-measured radial velocity as the radar scans along the approach path. Positive radial velocity is away from the radar.

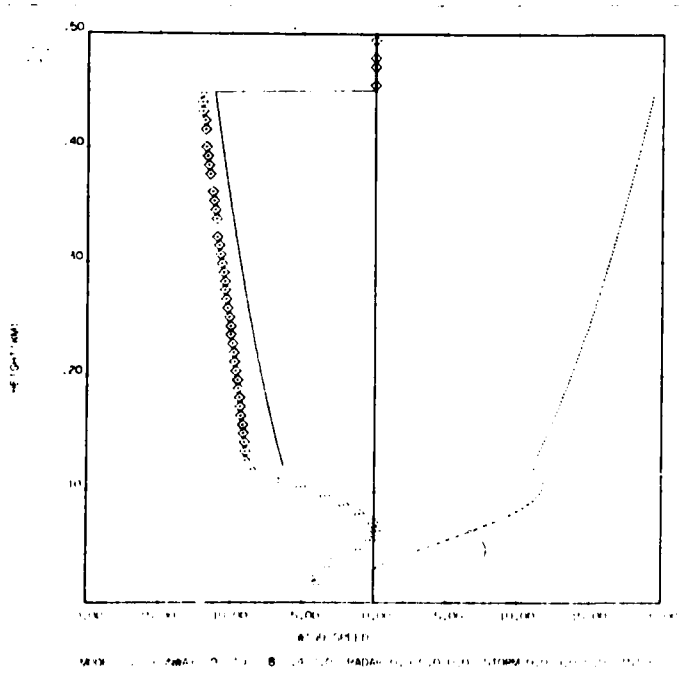

Figure 6.4.

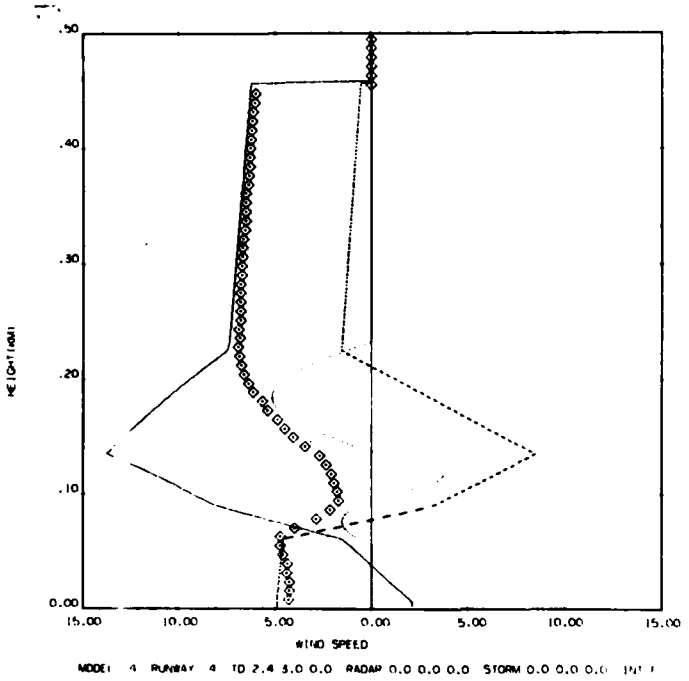

Figure 6.5.

WIND SPEED-HEIGHT PROFILES

Solid lines show headwinds (+) or tailwinds (-) encountered by a landing aircraft at various heights above touchdown. Dashed lines show crosswinds and dotted lines show vertical winds along the approach path. Positive crosswind causes a landing aircraft to drift to the right and positive vertical wind is upward. Diamond points are the expected value of radar-measured radial velocity as the radar scans along the approach path. Positive radial velocity is away from the radar.

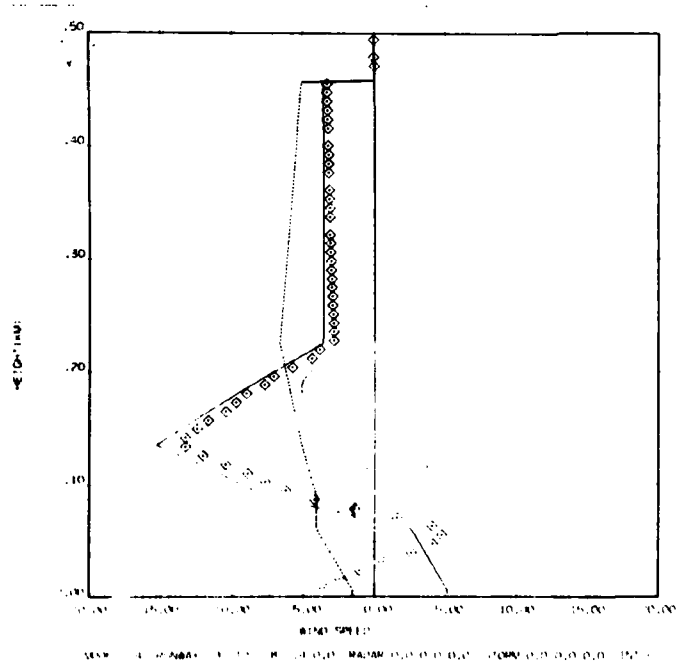

Figure 6.6.

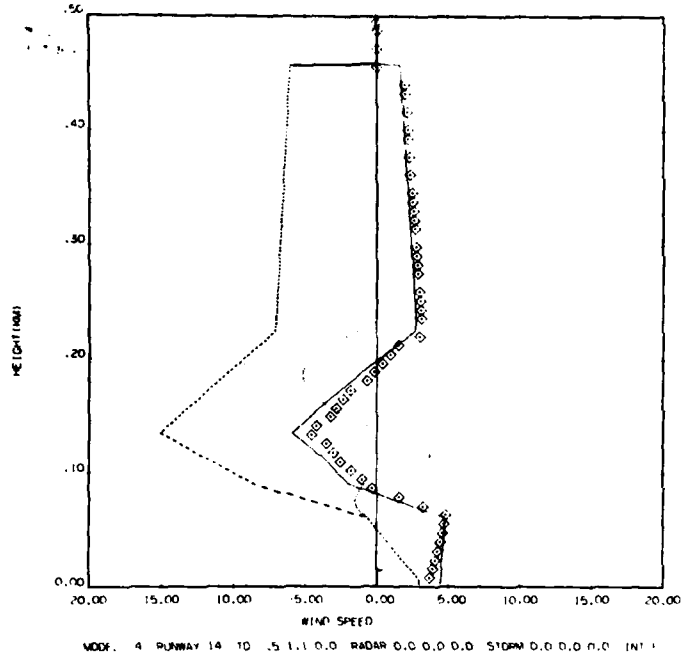

Figure 6.7.

WIND SPEED-HEIGHT PROFILES

Solid lines show headwinds (+) or tailwinds (-) encountered by a landing aircraft at various heights above touchdown. Dashed lines show crosswinds and dotted lines show vertical winds along the approach path. Positive crosswind causes a landing aircraft to drift to the right and positive vertical wind is upward. Diamond points are the expected value of radar-measured radial velocity as the radar scans along the approach path. Positive radial velocity is away from the radar.

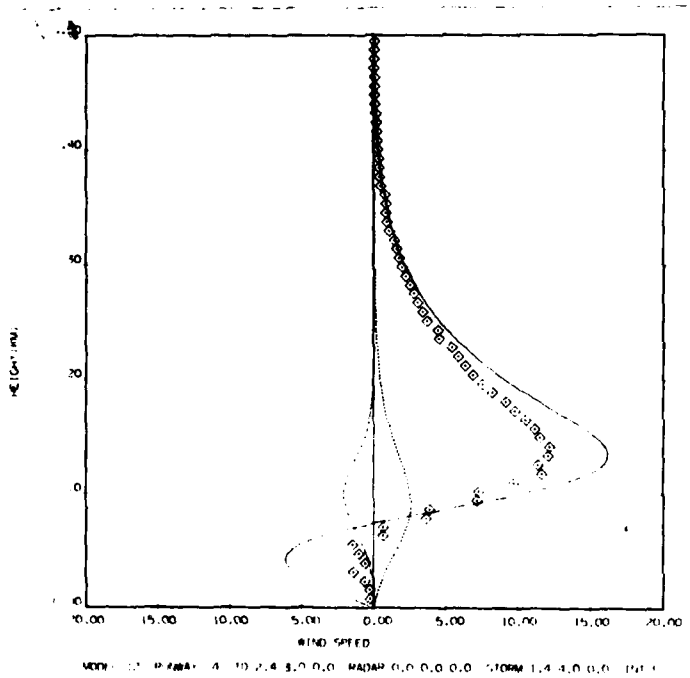

Figure 6.8.

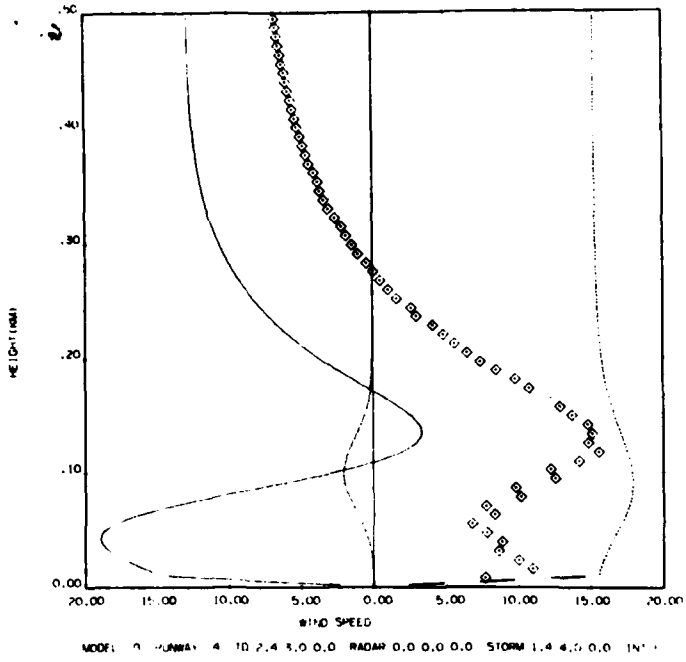

Figure 6.9.

WIND SPEED-HEIGHT PROFILES

Solid lines show headwinds (+) or tailwinds (-) encountered by a landing aircraft at various heights above touchdown. Dashed lines show crosswinds and dotted lines show vertical winds along the approach path. Positive crosswind causes a landing aircraft to drift to the right and positive vertical wind is upward. Diamond points are the expected value of radar-measured radial velocity as the radar scans along the approach path. Positive radial velocity is away from the radar.

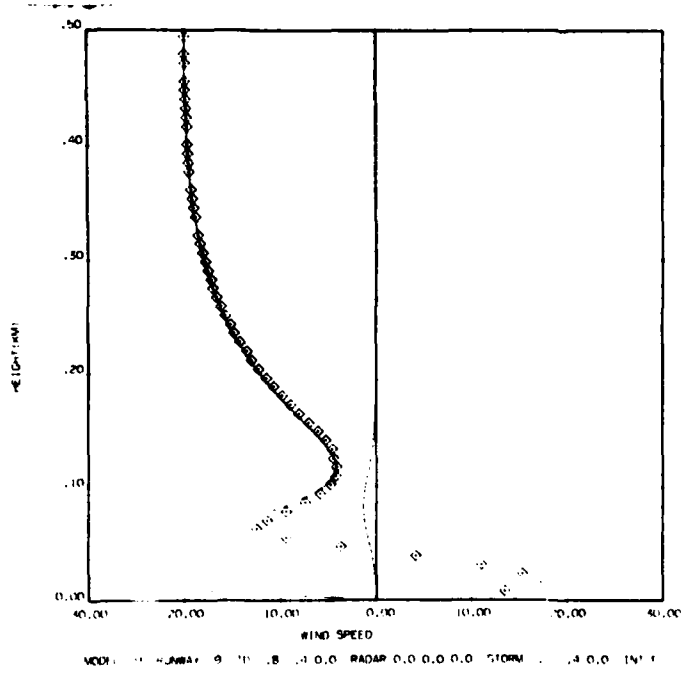

Figure 6.10.

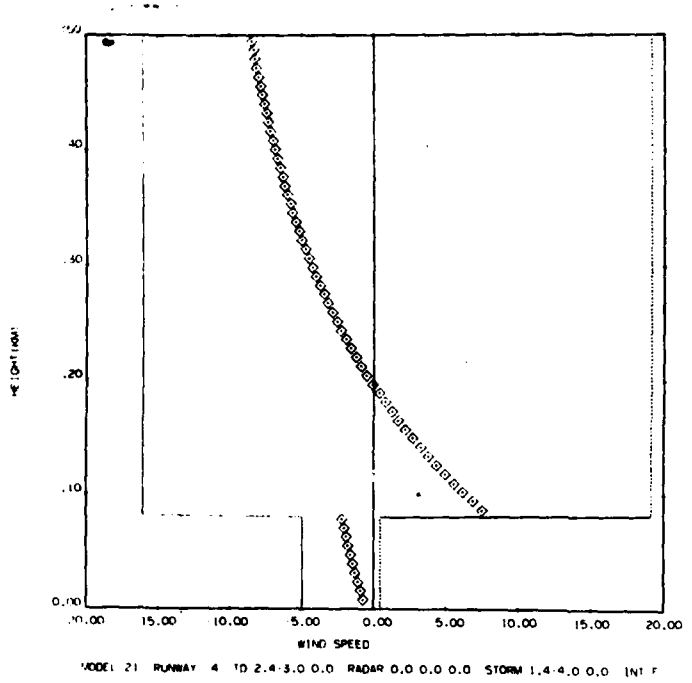

Figure 6.11.

WIND SPEED-HEIGHT PROFILES

Solid lines show headwinds (+) or tailwinds (-) encountered by a landing aircraft at various heights above touchdown. Dashed lines show crosswinds and dotted lines show vertical winds along the approach path. Positive crosswind causes a landing aircraft to drift to the right and positive vertical wind is upward. Diamond points are the expected value of radar-measured radial velocity as the radar scans along the approach path. Positive radial velocity is away from the radar.

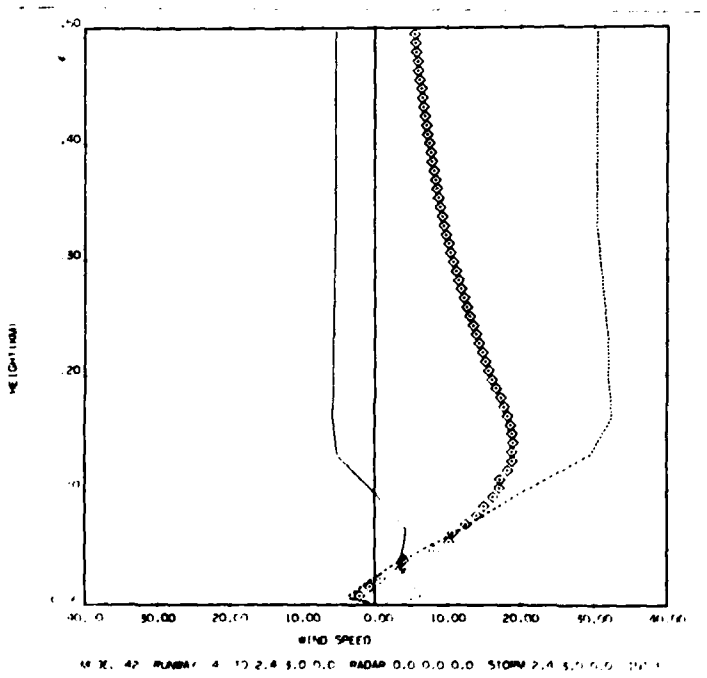

Figure 6.12.

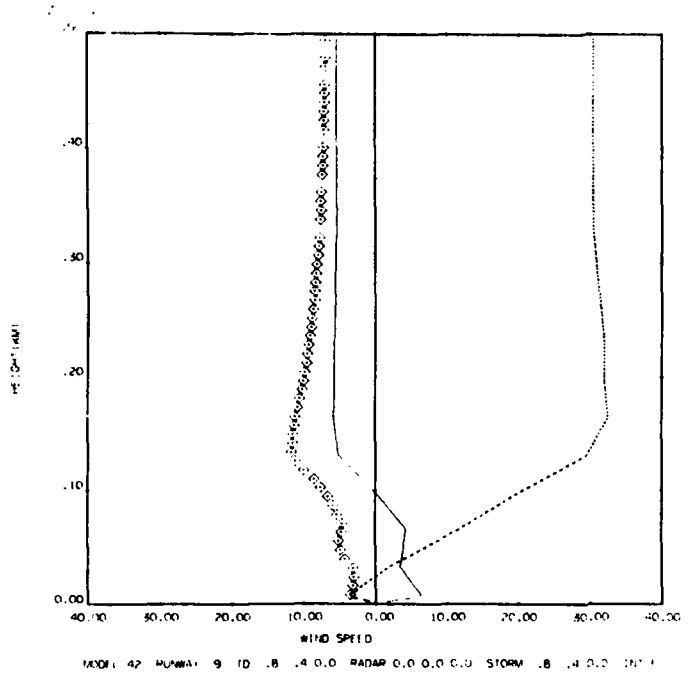

Figure 6.13.

WIND SPEED-HEIGHT PROFILES

Solid lines show headwinds (+) or tailwinds (-) encountered by a landing aircraft at various heights above touchdown. Dashed lines show crosswinds and dotted lines show vertical winds along the approach path. Positive crosswind causes a landing aircraft to drift to the right and positive vertical wind is upward. Diamond points are the expected value of radar-measured radial velocity as the radar scans along the approach path. Positive radial velocity is away from the radar.

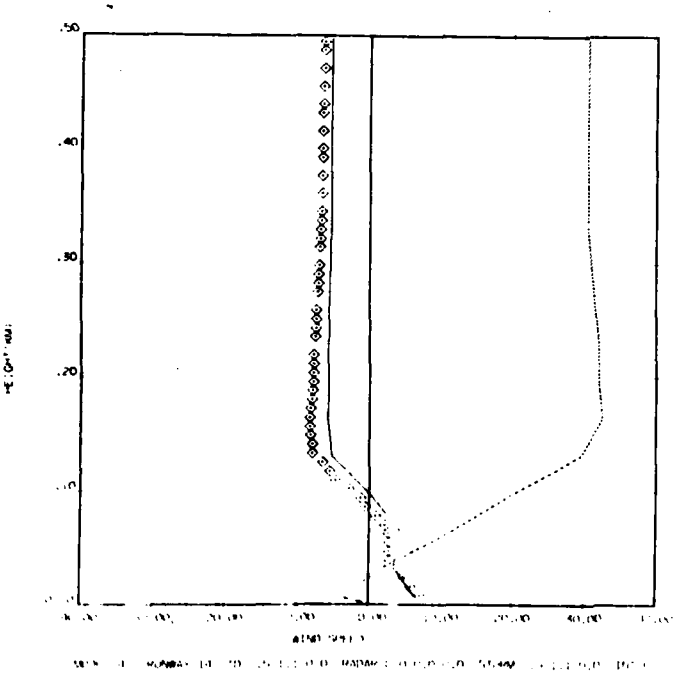

Figure 6.14.

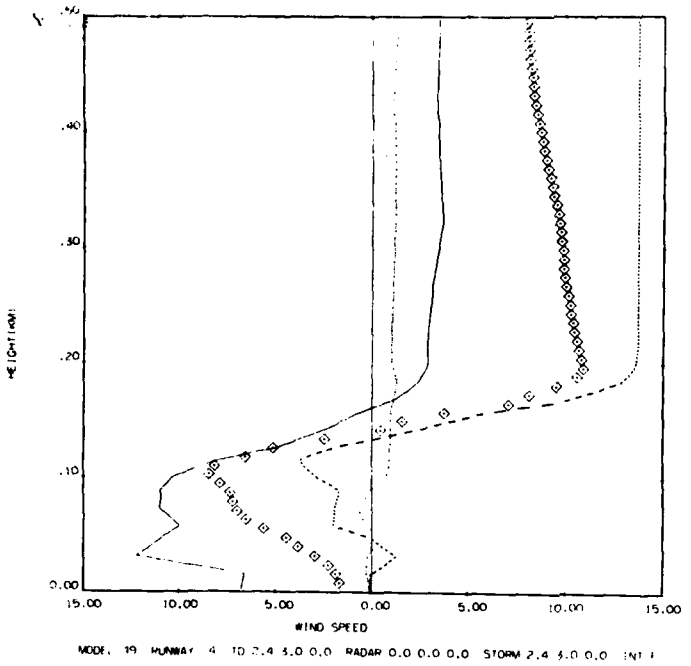

Figure 6.15.

WIND SPEED-HEIGHT PROFILES

Solid lines show headwinds (+) or tailwinds (-) encountered by a landing aircraft at various heights above touchdown. Dashed lines show crosswinds and dotted lines show vertical winds along the approach path. Positive crosswind causes a landing aircraft to drift to the right and positive vertical wind is upward. Diamond points are the expected value of radar-measured radial velocity as the radar scans along the approach path. Positive radial velocity is away from the radar.

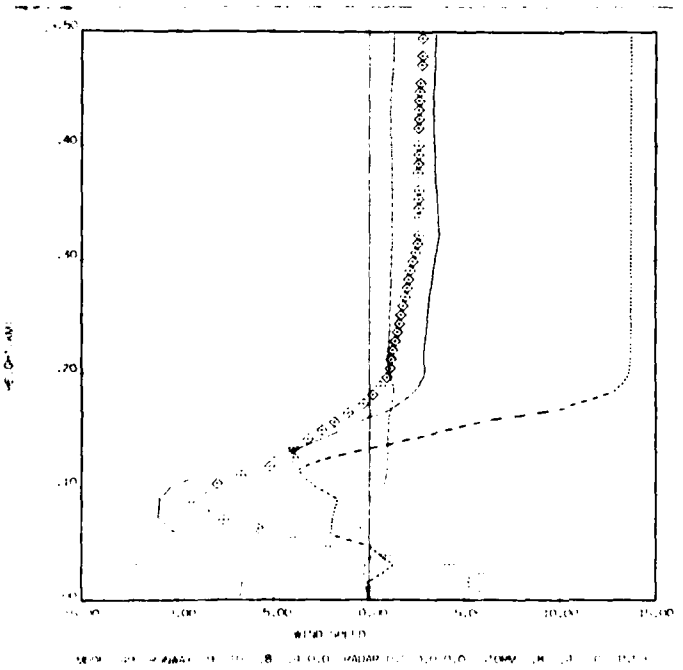

Figure 6.16.

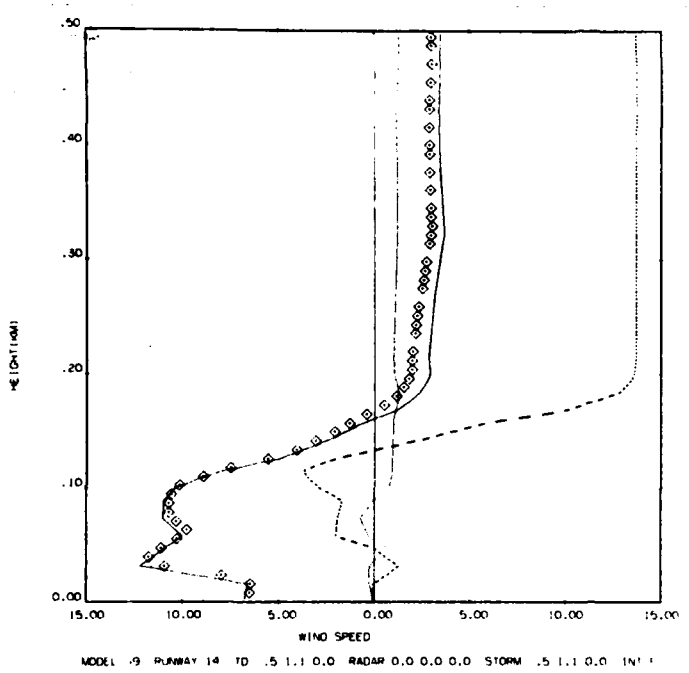

Figure 6.17.

WIND SPEED-HEIGHT PROFILES

Solid lines show headwinds (+) or tailwinds (-) encountered by a landing aircraft at various heights above touchdown. Dashed lines show crosswinds and dotted lines show vertical winds along the approach path. Positive crosswind causes a landing aircraft to drift to the right and positive vertical wind is upward. Diamond points are the expected value of radar-measured radial velocity as the radar scans along the approach path. Positive radial velocity is away from the radar.

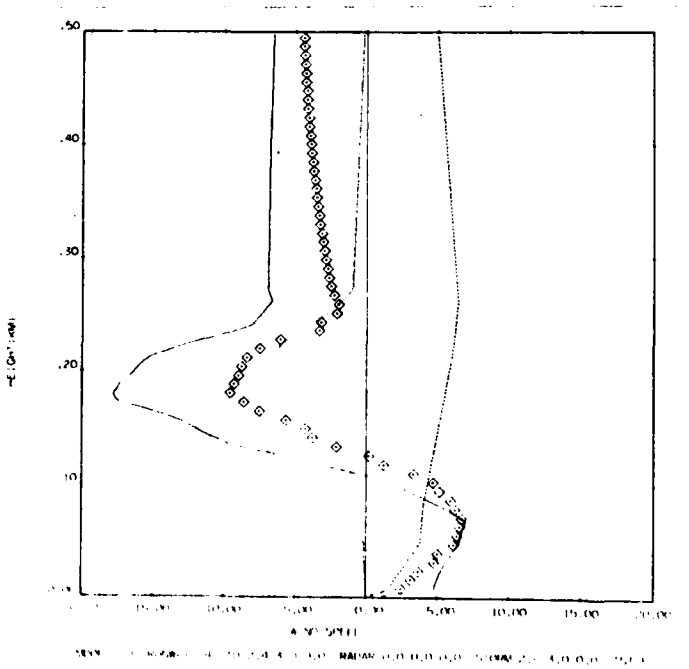

Figure 6.18.

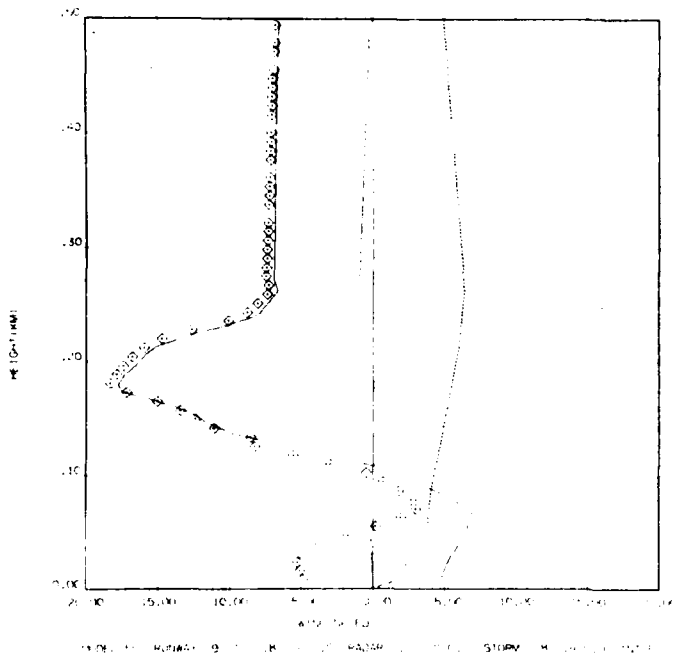

Figure 6.19.

WIND SPEED-HEIGHT PROFILES

Solid lines show headwinds (+) or tailwinds (-) encountered by a landing aircraft at various heights above touchdown. Dashed lines show crosswinds and dotted lines show vertical winds along the approach path. Positive crosswind causes a landing aircraft to drift to the right and positive vertical wind is upward. Diamond points are the expected value of radar-measured radial velocity as the radar scans along the approach path. Positive radial velocity is away from the radar.

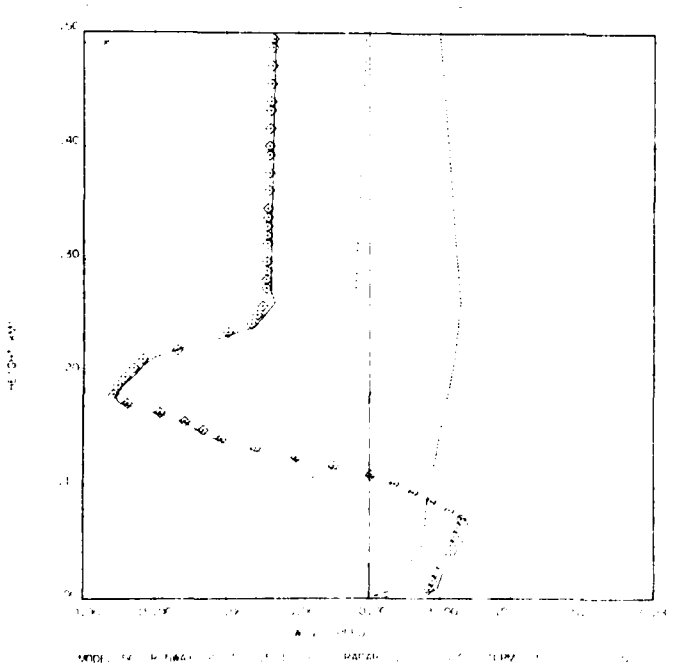

Figure 6.20.

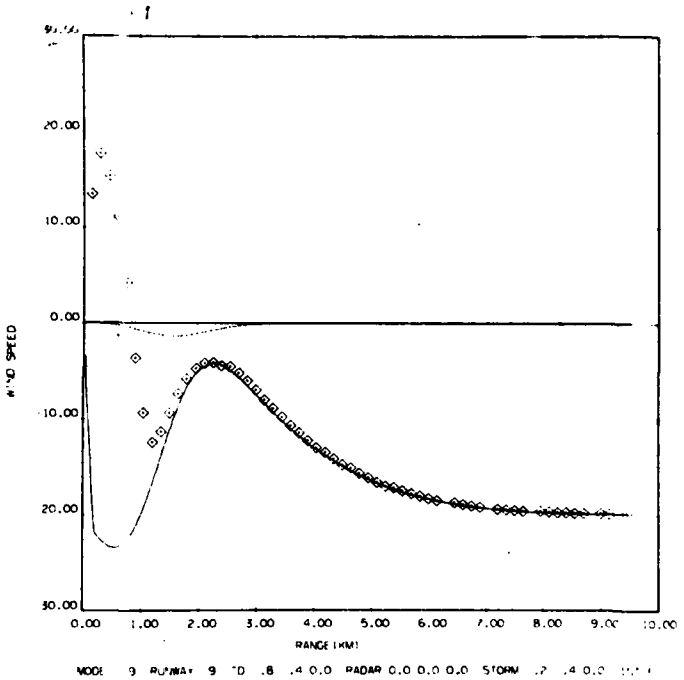

Figure 6.21.

Wind speed-range profile for model 9, Runway 9. Range is distance from touchdown. Data are same as shown in Fig. 6.10.

B. Radial Velocity Fields (Figures 6.22-6.39)

The three types of displays of the radial velocity fields near the approach path are illustrated in Fig. 6.22-6.24. Figure 6.22 shows contours of constant radial velocity ("isodops") for a fixed elevation angle (1.5 deg) which intersects the approach to [4] at about 250 m height. The scan is therefore a section of a VAD scan; however, instead of the conventional PPI presentation as in Fig. 4.1, where isodops are radial lines, the data presentation is a B-scan so the isodops for a uniform wind appear as straight lines normal to the azimuth axis. Heavy lines denote contour intervals of 10 m/s, light lines denote 5 m/s intervals. This scan intersects the approach path at only one point. Model 1, shown in Fig. 6.22 has large shear at very low altitudes which were not covered by the simulation scan so the contours are nearly those for uniform winds.

Figure 6.23 shows the isodops on a surface that includes the approach path. The approach path is shown with short vertical arrows; quantization with azimuth

and elevation increments of 0.1 deg causes the irregularities in the display. The display shows the isodops on a surface where the range and elevation angle of all points with constant altitude is the same as the range and elevation angle where the scan intersects the approach path. Since data are displayed as a function of azimuth, uniform winds will result in isodops that appear as vertical lines. The low level wind shear of model 1 is seen in Fig. 6.23 because the simulation scan covers the approach path at all heights below 500 m.

Another display which includes the approach path is shown in Fig. 6.24. In this case the antenna scans along the approach path so the data surface is a plane which includes the approach path, radar location, and touchdown point. At each azimuth angle where the radar beam intersects the approach path, the radial velocity is displayed as a function of range. Since all points along the range axis correspond to a fixed antenna position, the isodops for uniform winds will be horizontal lines. The altitude coordinate is the altitude on the approach path, not the altitude of all data points. The constant elevation angle scan and display (as in Fig. 6.22) would be the easiest to implement on an actual radar but it does not observe the winds along the aircraft track. The glide slope scan, (Fig. 6.24), could be implemented on any computer-controlled radar and the processing and display would be as easy to implement as for the constant elevation scan. The scan illustrated in Fig. 6.23 is not a practical scan for an actual radar since it displays only one range at any antenna position. The radial velocity fields shown for other wind models will therefore be the glide slope scan where uniform winds will have horizontal isodops.

The glide slope scans for [4], [9], and [14] using model 4 are shown in Figs. 6.25-6.27. The corresponding radial profiles are in Figs. 6.5-6.7. Although the isodops clearly indicate that the wind is not uniform, only for [9] do the contours show that the glide slope crosses a rapidly changing wind. This is consistent with the radial profiles which only show large gradients for [9].

Simulation results for downburst models (Figs. 6.28-6.30) show the rapid change in radial velocity along all 3 approach paths. Figure 6.28 shows the contours for [4] with a uniform wind from the west added to the downburst model and Fig. 6.29 shows the contours for [9] with a uniform wind from the

south added to the downburst. Figure 6.30 shows the downburst for [14]. The isodops are strongly dependent on the location of the downburst relative to touchdown but the vertical orientation of the contours show that the wind field is not uniform.

The glide slope scans for [4] using models 44, 49, and 50 and shown in Fig. 6.31-6.33. Though these wind models depict different meteorological situations (models 44 and 50 represent thunderstorms and model 49 represents a frontal passage), the basic characteristics of the radial velocity fields are very similar. Again, the isodops become oriented toward the vertical showing the changing wind field along the approach path. The same general character of the radial velocity fields are observed for the other runways. Figures 6.34-6.36 show the isodops for the same wind models on [9] and Figs. 6.37-6.39 show those for [14]. These scans suggest that the orientation of the isodops for a radar scan along the glide slope are a sensitive indicator of changing winds along the approach path.

One of the problems with the display used in Figs. 6.24-6.39 is that the resulting patterns of radial velocity are complex and difficult to interpret, even for relatively simple wind fields. A measurement and display technique that might be suitable for wind shear warning is as follows: First, use the radar to measure vertical profiles of the horizontal wind with the VAD scan or 4-point measurement. The winds are assumed to vary with height and linearly with horizontal distance. The radar then scans along the approach path and the measured radial velocities are compared with those that would be present if the radar-measured wind profile were applicable. The difference field is then displayed. If the difference field is less than some threshold value, the profile would be assumed to apply along the approach path. Areas where the difference field exceeded some threshold could simply be coded as a shaded area on a display. For example, using this technique only the 2 and 3-dimensional wind models would have a difference field. There would be no need for operator interpretation — the system would yield a wind profile and an indication of when that mean profile may be assumed to apply along a particular approach.

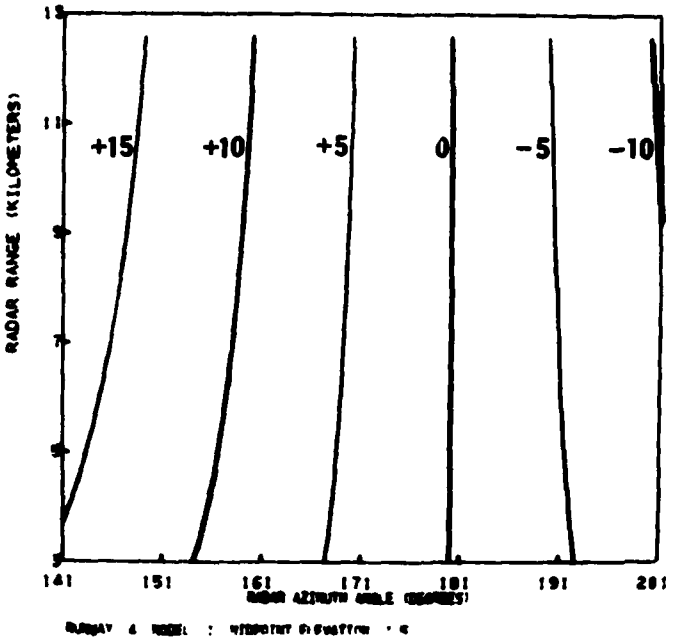

Figure 6.22.

Contours of constant radial velocity ("isodops") for a fixed antenna elevation angle scan. The scan intersects the glide path at only 1 point. Uniform winds would appear as vertical lines.

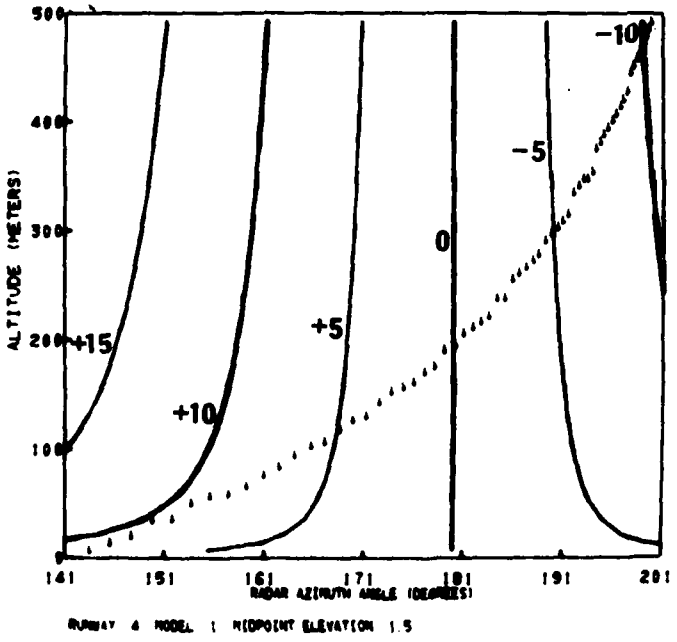

Figure 6.23.

Isodops on surface which includes the approach path, denoted by short vertical arrows. Radar range and antenna elevation angle at each altitude are the same as the range and elevation angle where the scan intersects the glide slope. Uniform winds appear as vertical lines.

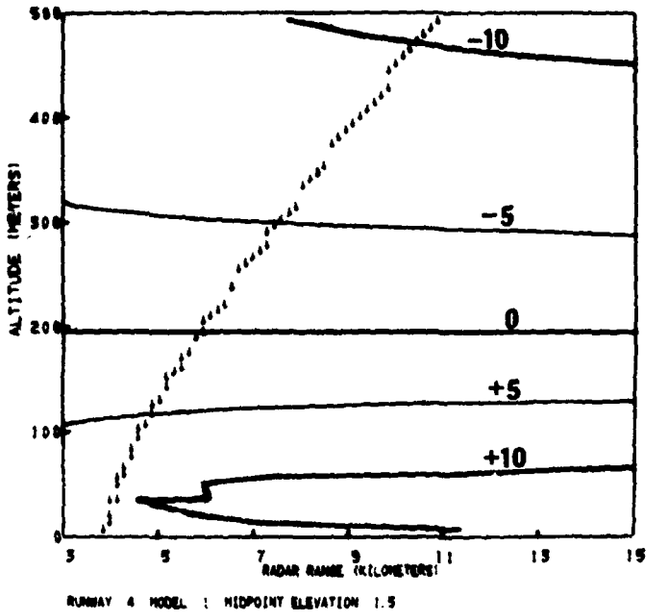

Figure 6.24.

Contours of constant radial velocity in a slant plane which includes the glide slope (shown by short vertical lines), the location of the radar, and the touchdown point. Uniform winds appear as horizontal lines because all points along the range axis (at fixed altitude) are measured at a fixed azimuth angle. The altitude coordinate shows the altitude on the approach path but not the altitude of all data points. Heavy lines are 10 m s^{-1} contour intervals; light lines are 5 m s^{-1} intervals.

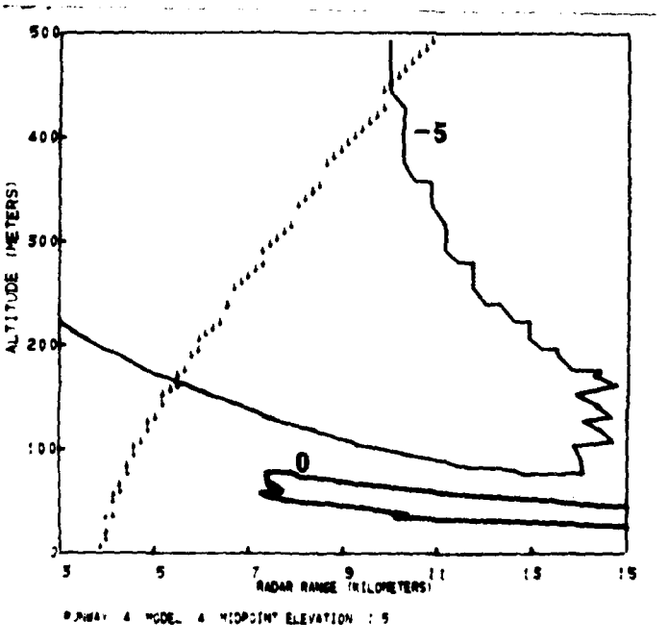

Figure 6.25.

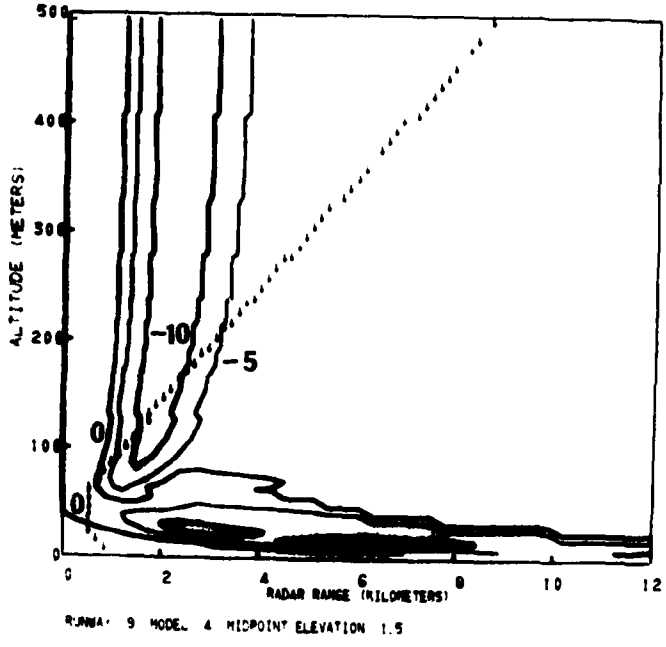

Figure 6.26.

Contours of constant radial velocity in a slant plane which includes the glide slope (shown by short vertical lines), the location of the radar, and the touchdown point. Uniform winds appear as horizontal lines because all points along the range axis (at fixed altitude) are measured at a fixed azimuth angle. The *altitude coordinate* shows the altitude on the approach path but not the altitude of all data points. Heavy lines are 10 m s^{-1} contour intervals; light lines are 5 m s^{-1} intervals.

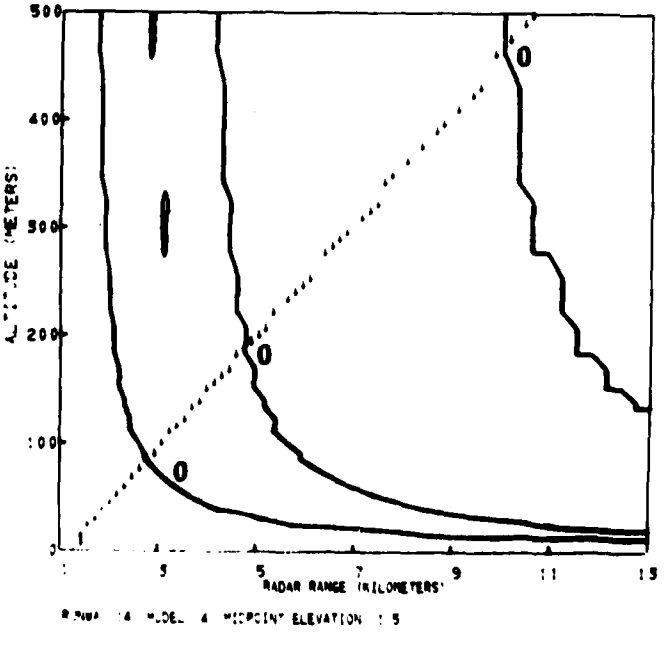

Figure 6.27.

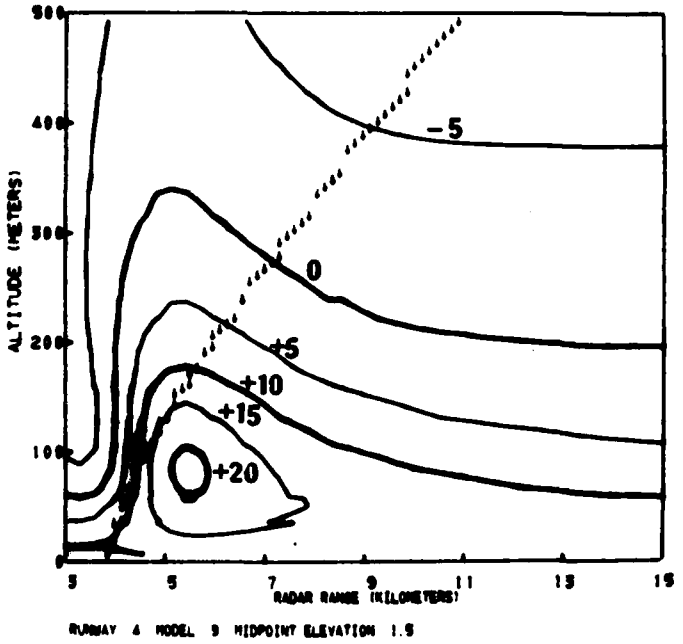

Figure 6.28.

Contours of constant radial velocity in a slant plane which includes the glide slope (shown by short vertical lines), the location of the radar, and the touchdown point. Uniform winds appear as horizontal lines because all points along the range axis (at fixed altitude) are measured at a fixed azimuth angle. The altitude coordinate shows the altitude on the approach path but not the altitude of all data points. Heavy lines are 10 m s^{-1} contour intervals; light lines are 5 m s^{-1} intervals.

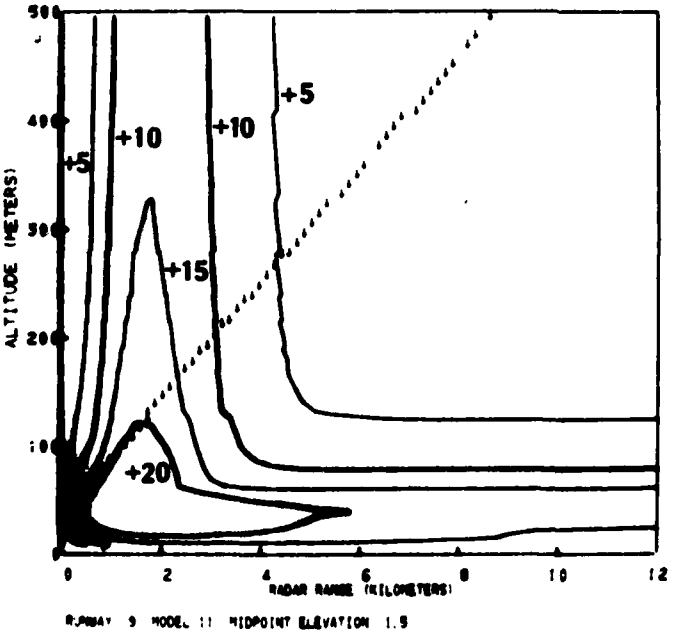

Figure 6.29.

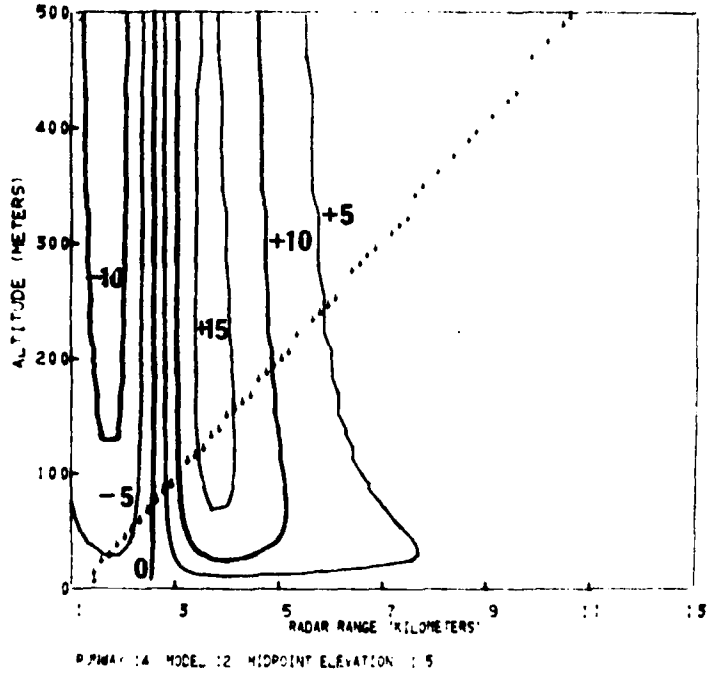

Figure 6.30.

Contours of constant radial velocity in a slant plane which includes the glide slope (shown by short vertical lines), the location of the radar, and the touchdown point. Uniform winds appear as horizontal lines because all points along the range axis (at fixed altitude) are measured at a fixed azimuth angle. The altitude coordinate shows the altitude on the approach path but not the altitude of all data points. Heavy lines are 10 m s^{-1} contour intervals; light lines are 5 m s^{-1} intervals.

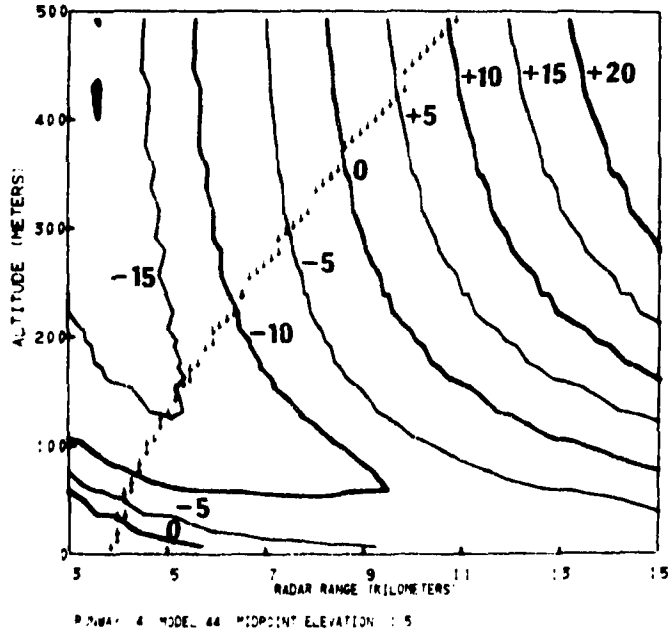

Figure 6.31.

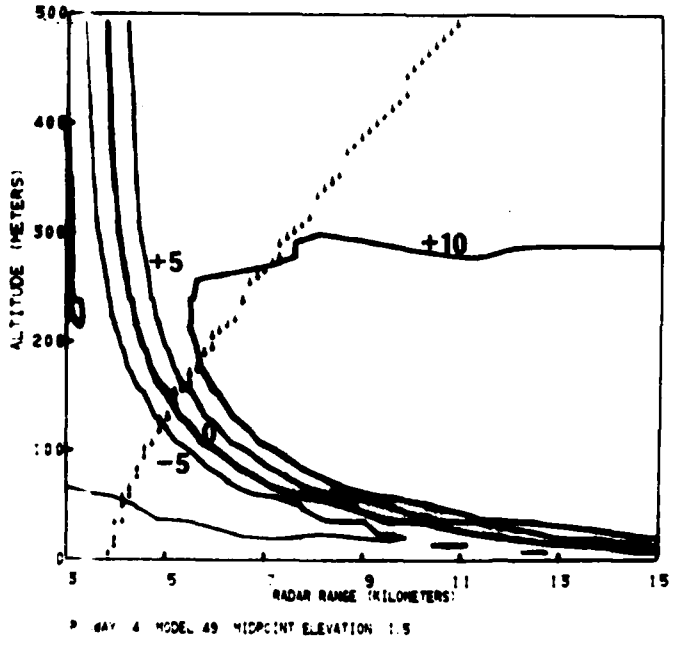

Figure 6.32.

Contours of constant radial velocity in a slant plane which includes the glide slope (shown by short vertical lines), the location of the radar, and the touchdown point. Uniform winds appear as horizontal lines because all points along the range axis (at fixed altitude) are measured at a fixed azimuth angle. The altitude coordinate shows the altitude on the approach path but not the altitude of all data points. Heavy lines are 10 m s^{-1} contour intervals; light lines are 5 m s^{-1} intervals.

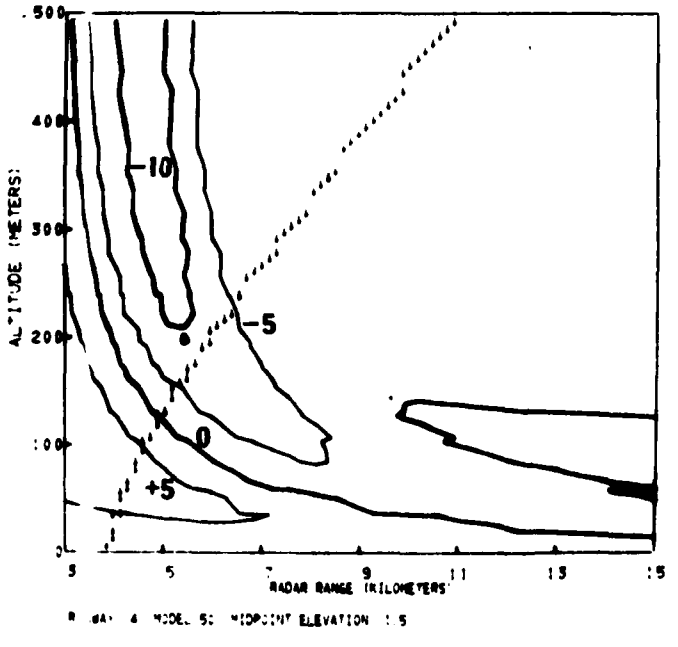

Figure 6.33.

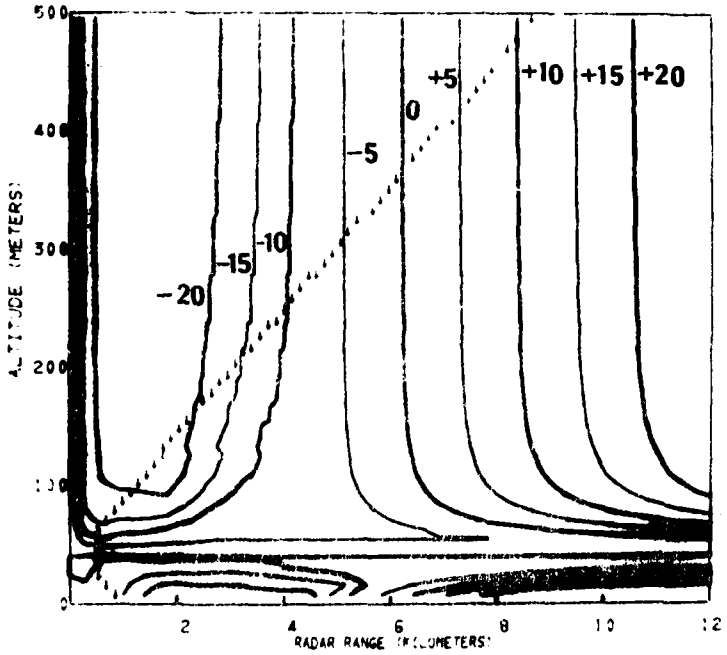

Figure 6.34.

Contours of constant radial velocity in a slant plane which includes the glide slope (shown by short vertical lines), the location of the radar, and the touchdown point. Uniform winds appear as horizontal lines because all points along the range axis (at fixed altitude) are measured at a fixed azimuth angle. The altitude coordinate shows the altitude on the approach path but not the altitude of all data points. Heavy lines are 10 m s^{-1} contour intervals; light lines are 5 m s^{-1} intervals.

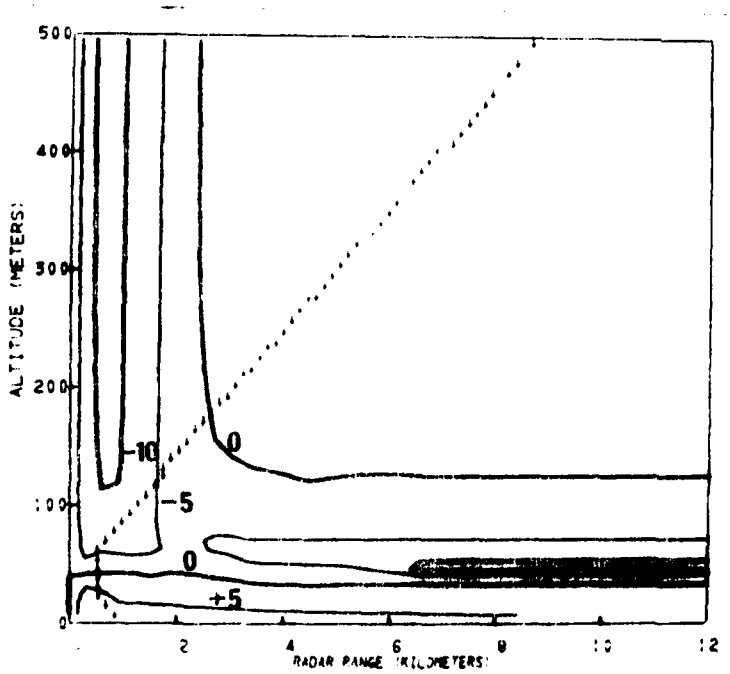

Figure 6.35.

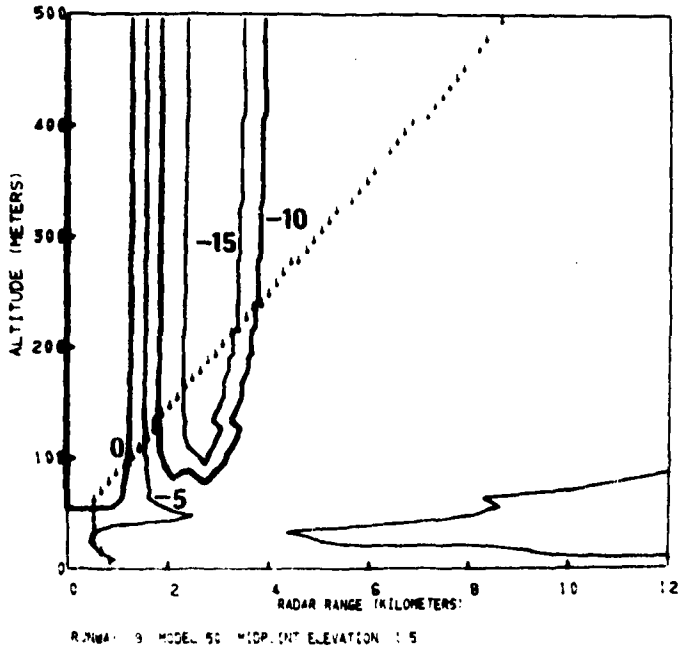

Figure 6.36.

Contours of constant radial velocity in a slant plane which includes the glide slope (shown by short vertical lines), the location of the radar, and the touchdown point. Uniform winds appear as horizontal lines because all points along the range axis (at fixed altitude) are measured at a fixed azimuth angle. The altitude coordinate shows the altitude on the approach path but not the altitude of all data points. Heavy lines are 10 m s^{-1} contour intervals; light lines are 5 m s^{-1} intervals.

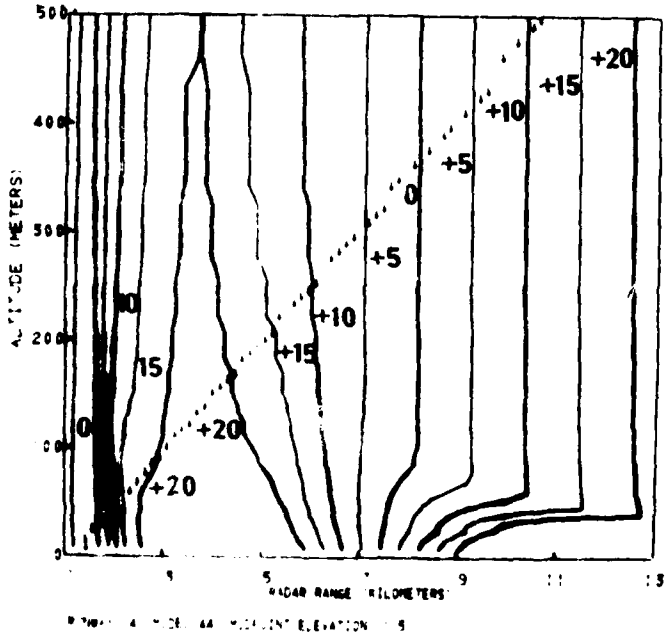

Figure 6.37.

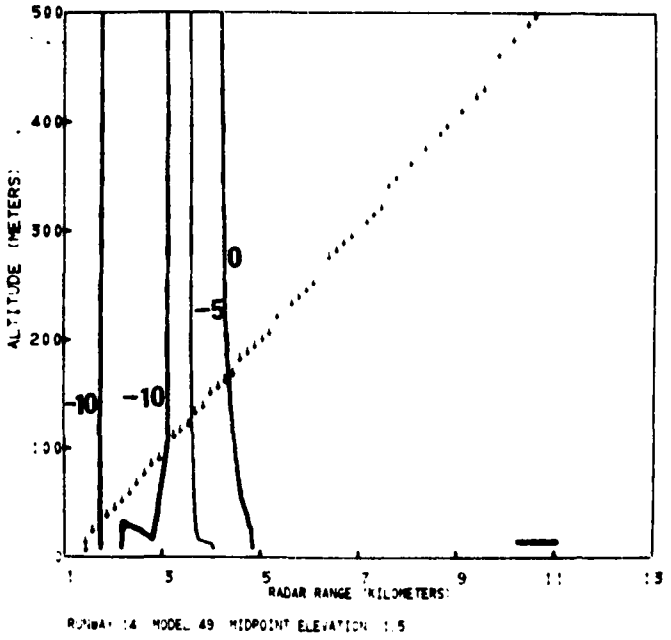

Figure 6.38.

Contours of constant radial velocity in a slant plane which includes the glide slope (shown by short vertical lines), the location of the radar, and the touchdown point. Uniform winds appear as horizontal lines because all points along the range axis (at fixed altitude) are measured at a fixed azimuth angle. The altitude coordinate shows the altitude on the approach path but not the altitude of all data points. Heavy lines are 10 m s^{-1} contour intervals; light lines are 5 m s^{-1} intervals.

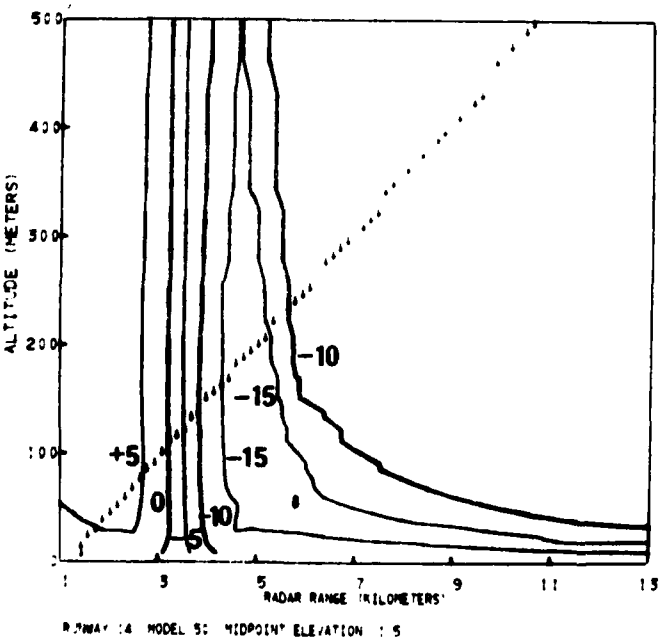

Figure 6.39.

8. CONCLUSIONS AND RECOMMENDATIONS

The major objectives of the NOAA-FAA program for investigating the use of pulse Doppler radar for wind shear warning at airports were to: (a) demonstrate, with modifications to existing FAA radars, that pulse Doppler radar can be used to measure winds in the optically clear air as well as in precipitation. (b) Explore the limitations of Doppler radar as a wind shear detector, and (c) determine how a single Doppler radar should be used for wind shear detection.

Experimental work at NAFEC with an ASR-8 radar equipped with a 15 foot diameter parabolic antenna has demonstrated that the radial wind component can be measured in various weather conditions. There has not been sufficient experimental evidence to show that this radar can measure the wind in <u>all</u> weather conditions, particularly in the clear air during the winter months when radio refractive turbulence is decreased. The experimental work has been limited to measuring radial wind profiles; vertical profiles of the horizontal wind and radial velocity fields have not been measured. The existing hardware at NAFEC is sufficient to perform these tests. Measurements of wind profiles can be made with the data system used for the wind shear program, and measurements of radial velocity fields (scanning antenna) can be made with the data system that was developed for storm turbulence detection.

In order to fully exploit the ASR-8 system at NAFEC as a <u>real-time</u> wind measurement system the data rate needs to be increased so that about 32 range intervals could be measured simultaneously. This would require a Fast Fourier Transform (FFT) array processor for the minicomputer system. A color display and multi-moment display would also be needed. While the present system is sufficient for verifying potential capability with off-line processing and limited real-time processing, it lacks the features required for an operational demonstration. If the FAA decides to continue to pursue the use of existing radars for weather information, then real-time capability will have to be added for both wind shear and storm turbulence work. The role of existing radars depends on the role that new generation weather radars (NEXRAD) will have for airport meteorology. A NEXRAD radar, if suitably located and devoted to airport surveilance, could provide storm surveilance and storm turbulence

indications for the terminal controllers. The radar would probably be sufficiently remote from the landing area so the airport itself would not be in the clutter pattern. This would preclude its use for wind measurements with useful height resolution, but it would be an important part of a wind shear warning system because it would monitor storms as they approach the airport. Another radar located at the airport and solely devoted to wind measurements would be one possible solution to the airport weather problem.

Simulation results show that a radar with a 150 m range resolution and a 1.5 deg beamwidth, located at the airport, is capable of resolving low-level wind profiles that are hazardous to aircraft during landing or takeoff. Vertical profiles of the horizontal wind at the radar site can be measured with an antenna elevation angle of 3 to 10 deg. It should be possible to measure the profile to several hundred meters altitude in all-weather conditions, and much higher in precipitation. Whether the wind profile at the radar is the profile that will be encountered along the aircraft track can be tested by measuring the radial velocity profile along the glide path and comparing it with the expected profile based on the measured vertical profile of horizontal wind. A suitably located radar could measure headwind profiles along one or more approach paths. [If measurement of headwind along the actual approach path is sufficient for a wind shear warning system, an alternative to a single radar devoted to wind shear would be to have several transmitter-antennas served by a single data system so that the headwinds could be monitored along all approach and departure paths. The sensitivity of each radar would not have to be as great, the antennas would be stationary and such a system could be competitive in cost. An FM-CW radar could be considered for this application.]

A single Doppler radar cannot measure the actual wind along the approach path in the complex meteorological situations associated with convective storms. In this case the radar can only infer wind shear from the measurement of the radial velocity and its gradients along the approach path and the surrounding area. It should be noted that vertical winds cannot be measured along the approach path by a Doppler radar since the elevation angles will be too low to sense a significant component of vertical motion. Detection of dangerous vertical winds must be indirect — that is, their presence must be sensed by the

perturbations (divergence) of the accompanying horizontal flow. Simulations show that wind shear can be detected by a scanning Doppler radar. The simulations used did not investigate whether every wind shear could be detected from radial velocity measurements but it did show that shear in specific models used to depict dangerous winds could be detected.

A shear detection and display technique for operational use is suggested for a single Doppler radar which is located so that it cannot observe headwinds on all approach paths. It would measure wind profiles which are assumed to apply only at the radar location. (The temporal changes in these profiles are one indication of the lateral extent of their validity.) The radar would then compare the radial velocity measurements made by scanning the area around the approach path with those expected from the profile measurements. If the measurements agreed the profile would be assumed to be valid along the approach path. If they did not agree (within specified limits), then the wind profile would not apply and the area could be shown simply on a control display as a region of wind shear caused by horizontal wind gradients. This type of display and warning system could be investigated further using the computer programs developed for the work reported here.

9. REFERENCES

1. Fujita, T. T., and F. Caracena, (1977), "An analysis of three weather-related aircraft accidents," Bull. Amer. Meteorol. Soc., Vol. 58, pp. 1164-1181.

2. Bedard, A. J., W. H. Hooke, and D. W. Beran, (1977), "The Dulles Airport pressure jump detector array for gust front detection," Bull. Amer. Meteorol. Soc., Vol. 58, pp. 920-926.

3. Goff, R. C., and E. E. Schlatter, (1978), "An operational application of mesonetworks for warning of translating surface wind change boundaries," presented at the 4th Symp. on Meteorol. Observations and Instrumen., Denver, CO., Apr. 10-14.

4. Hardesty, R. M., P. A. Mandics, D. W. Beran, and R. G. Strauch, (1977), "The Dulles Airport acoustic-microwave radar wind and wind shear measuring system," Bull. Amer. Meteorol. Soc., Vol. 58, pp. 910-918.

5. Kalafus, R. M., (1978), "Wind shear requirements and their application to laser systems," U.S. Dept. of Transportation Rep. FAA-RD-77-123, 140 pp.

6. "Final Report on the Joint Doppler Operational Project (JDOP) 1976-1978." NOAA Tech. Memo. ERL NSSL-86, 84 pp.

7. Doviak, R. J., and M. Berger, (1979), "Turbulence and waves in the optically clear air planetary boundary layer resolved by dual Doppler radars," Rad. Sci., in press.

8. Chadwick, R. B., K. P. Moran, R. G. Strauch, G. E. Morrison, and W. C. Campbell, (1976), "Microwave radar wind measurements in the clear air," Rad. Sci., Vol. 11, pp. 795-802.

9. Chadwick, R. B., K. P. Moran, G. E. Morrison, and W. C. Campbell, (1978), "Measurements showing the feasibility for radar detection of hazardous wind shear at airports," Final Report, AFGL-TR-78-0160, 49 pp.

10. Offi, D. L., and W. Lewis, (1978), "Preliminary tests of the ASR-8 wind shear detection system," NAFEC Tech. Letter Report NA-78-59-LR.

11. Offi, D. L., W. Lewis, T. Lee, and A. DelaMarche, (1980), "Test and evaluation of the ASR-8 Wind Shear Detection System," U.S. Dept. of Transportation, Interim Report FAA-RD-80-21 (in press).

12. Sweezy, W. B., W. R. Moninger, and R. G. Strauch, (1978), "Simulation of radar-measured Doppler velocity profiles in low-level wind shear," U.S. Dept. of Transportation Rep. FAA-RD-78-46, 48 pp.

13. Lhermitte, R. M., and D. Atlas, (1961), "Precipitation motion by pulse Doppler radar," Proc. 9th Weather Radar Conf., Boston, MA, pp. 218-233.

14. Browning, K. A., and R. Wexler, (1968), "The determination of kinematic properties of a wind field using Doppler radar," J. Appl. Meteor., 7, 105-113.

15. Atlas, D., R. C. Srvastava, and R. S. Sekhon, (1973), "Doppler radar characteristics of precipitation at vertical incidence," Revs. of Geophys. and Space Phys., 11, pp. 1-35.

16. Rinehart, R. E., and E. T. Garvey, (1978), "Internal storm motions determined from radar reflectivity factor data," 18th Radar Meteor. Conf., Preprints, Amer. Meteor. Soc., Atlanta, GA, pp. 511-514.

17. Doviak, R. J., and M. Berger, (1979), "Turbulence and waves in the optically clear air planetary boundary layer resolved by dual Doppler radars," Rad. Sci. (in press).

18. Easterbrook, C. E., (1975), "Estimating horizontal wind fields by two-dimensional curve fitting of single Doppler radar measurements," 16th Radar Meteor. Conf., Preprints, Amer. Meteor. Soc., Houston, TX, pp. 214-219.

19. Waldteufel, P., and H. Corbin, (1979), "On the analysis of single-Doppler radar data," J. Appl. Meteor., Vol. 18, pp. 532-542.

20. Kraus, M. J., and R. Donaldson, (1976), "Interpretation of PPI velocity displays in widespread storms," 17th Radar Meteor. Conf. Preprints, Am. Meteorol. Soc., Seattle, WA, pp. 239-243.

21. Burgess, D. W., L. O. Hennington, R. J. Doviak, and P. S. Ray, (1976), "Multimoment Doppler display for severe storm identification," J. Appl. Meteorol., Vol. 15, pp. 1302-1306.

22. Fichtl, G. H., and D. W. Camp., letter to F. Melewicz dated Jan. 23, 1976.

23. Langweil, L., FAA memo dated Feb. 17, 1976.

APPENDIX: COMPUTER SIMULATION PROGRAM

The structural diagram for the expanded simulation program is given in Fig. A.1, and the associated input-output table is Table A.1[12]. The program has been expanded to simulate radar scanning, to display 3-dimensional wind components, and to include several additional wind models. In addition, some modifications were made in an attempt to make the program somewhat more simple and more efficient. For example, some of the modules were combined to eliminate redundancy, some parameters that were input previously (such as radar beam width and glide path angle) are now defined as constants, and some parameters that were passed through several levels of hierarchy are in a COMMON block.

In the fixed beam simulation used in Phase I, the origin of the Cartesian coordinate system was taken as the touchdown point[12]. In the present study, however, it was desirable to have the same radar scan several different runways, so that a more natural choice for origin is the radar location. The expanded program allows for a completely arbitrary coordinate system, including the possibility of the radar and runways being at different altitudes.

The following parameters: touchdown coordinates, XT, YT, ZT; the radar coordinate, XR, YR, ZR; the wind reference coordinates, XC, YC, ZC; the runway number, NRW (for aircraft heading); and a flag INTP to select radar radial velocities either at a point or integrated over pulse volume, are passed by the COMMON block, POSIT. In the current program INTP is also used to determine if a volume containing the glide path is scanned (point velocity option) or a scan intersecting the glide path issued (integrated velocity option). The wind reference coordinates are used to locate the center of the downburst models or an arbitrary point on the shear line for those particular models.

As in Phase I the model number MDN is passed by COMMON/MODEL/ and the specialized graphics routines are omitted from this discussion. Due to the length of the expanded program it is impractical to include a complete computer program listing in this report, but it is available from the authors upon request.

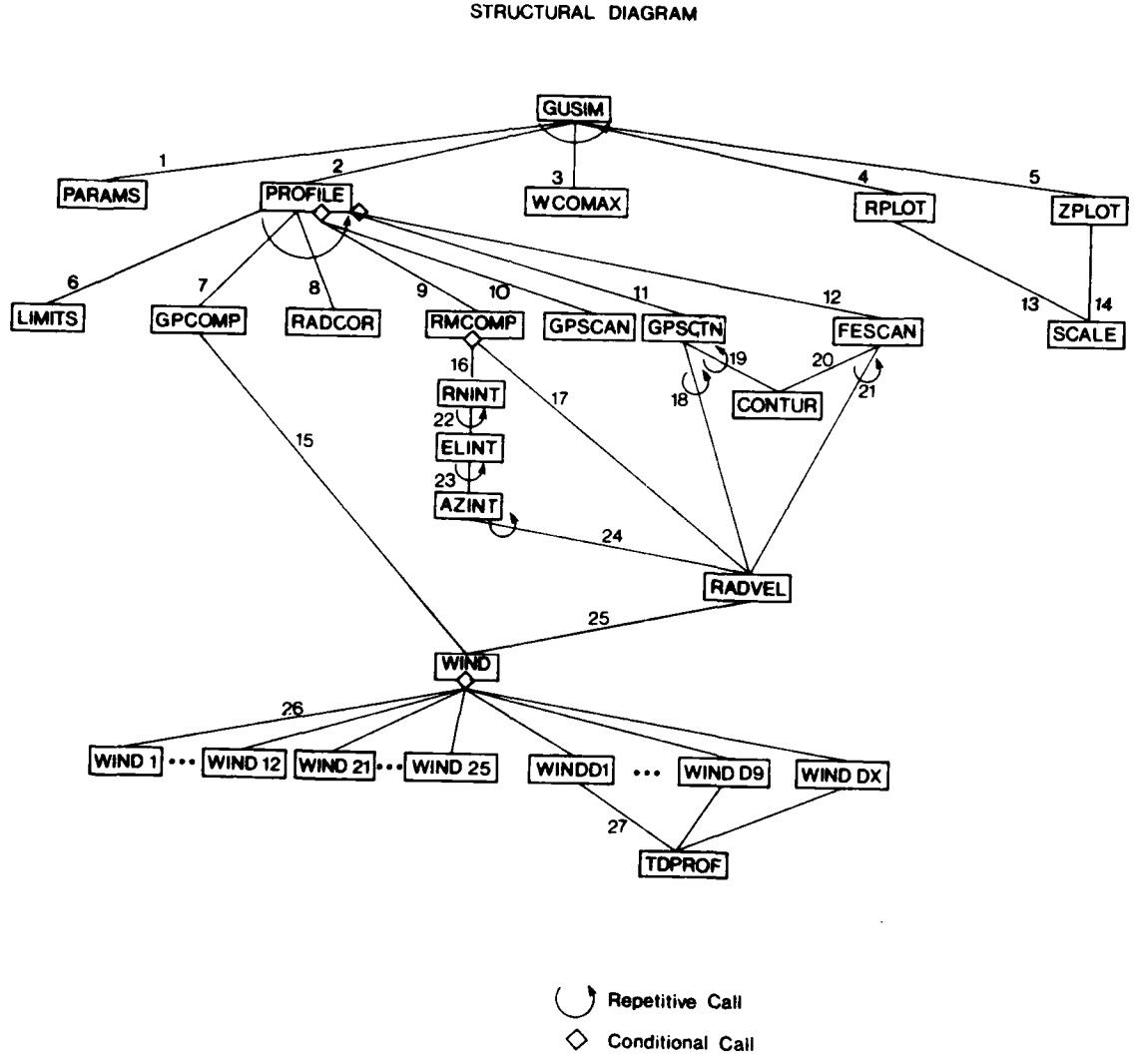

Figure A.1. Computer simulation program structural diagram.

Module description

GUSIM	-	driver that initializes, controls and terminates program execution.
PARAMS	-	reads in parameters for each approach and radar scan.
PROFILE	-	computes Cartesian coordinates along glide path for radar scan and controls scan and velocity contour plots.
WCOMAX	-	determines maximum wind component for profile plot scaling.
RPLOT	-	plots wind component velocity profiles as a function of aircraft range (distance from touchdown).
ZPLOT	-	plots wind component velocity profiles as a function of aircraft altitude.
LIMITS	-	determines limits and grid spacing for velocity contour plots.
GPCOMP	-	computes actual wind velocity components along glide path.
RADCOR	-	transforms Cartesian coordinates into spherical radar coordinates for radar scan.
RMCOMP	-	computes radar radial wind velocity components along the glide path.
GPSCAN	-	computes radial velocity components for radar scanning a volume that contains the glide path.
GPSCTN	-	contours radar radial velocity fields as a function of radar azimuth and aircraft height and as a function of radar range and aircraft height; and plots the glide path on each contour plot.
FESCAN	-	computes and contours the radial velocity field as a function of radar range and azimuth at a fixed elevation angle that intersects the glide path at about 5 km from touchdown.
SCALE	-	scales the profile plots.
RNINT	-	computes the radar-measured mean radial velocity within a pulse volume by integrating in range the mean radial velocity in the beam cross section.
CONTUR	-	scales and draws contour plots.
ELINT	-	computes the mean radial velocity in a beam cross section by integrating with respect to elevation the mean radial velocity in the azimuth beamwidth.

AZINT - computes the mean radial in the azimuth beamwidth.

RADVEL - converts the spherical coordinates to Cartesian and computes the radial component of u, v, and w.

WIND - provides decision table for selecting wind model.

WIND(N) - computes the wind components u, v, and w at the point (x,y,z) for wind model N (N=1, ... , 12, 21, ... , 25, D1, ... ,DX).

TDPROF - interpolates the numerical models 41 through 50 to the point (x,y,z) and transforms components to u,v,w.

The routines WINDD1 through WINDDX are for models 41 through 50.

INPUT-OUTPUT TABLE

INTER-FACE	INPUT	OUTPUT
1		MDN Model number
2		GPW Headwind component GPC Crosswind component GPV Vertical wind component GRG Distance from touchdown GPZ Aircraft altitude NCP Number of points in glide path profile RMW Radar radial wind velocity along glide path NRM Number of points in radar wind profile
3	GPW, GPC, GPV, NGP, RMW, NRM	WMX Absolute maximum wind velocity component
4	WMX, GPW, GPC, GPV, GPR, NGP, RMW, NRM	
5	WMX, GPW, GPG, GPV, GPZ, NGP, RMW, NRM	
6	CSEA Array of sines and cosines of glide path azimuth and elevation angle GPR RMN Minimum radar range NA Number of radar azimuth (and range) points in volume scan	ELM Mid-point elevation angle AA Radar azimuth grid points RA Radar range grid points
7	X, Y, Z Cartesian coordinate of the point CSEA	GPW, GPC, GPV At the point
8	X, Y, Z RMN DRM	RR Radar range REL Radar elevation angle RAZ Radar azimuth
9	RR, REL, RAZ, DRM DRR Range integration increment BW Radar beamwidth	RMW At a point

10	RR, REL, RAZ, RA, AA, NA NH Number of height increments in the radar scan	AG Radar azimuth of the scan and glide path intersection EG Radar elevation angle of the intersection RG Radar range of the intersection RZ Height of the center of pulse volume nearest the glide path VRA Radial velocity matrix as a function of height and azimuth VRR Radial velocity matrix as a function of height and range
11	AA, RZ, AG, NA, NM VR is VRA or VRR KT Scan type indicator	
12	RA, ELM, AA NR Number of range steps in radar scan	VRA Radial velocity matrix as a function of azimuth and height
13	WMX	YUP Maximum y-axis value YLO Minimum y-axis value KDY Number of y-axis grid divisions
14	WMX	XUP Maximum x-axis value XLO Minimum x-axis value KDX Number of x-axis grid divisions
15	X, Y, Z	U,V,W Cartesian wind components
16	EE, REL, RAZ, DRR, DRM	Mean radial velocity within the pulse volume
17	RR, REL, RAZ	Radial velocity at a point
18	R is RA or RR AZ is AA or RAZ REL	Radial velocity at a point
19	AA, RZ, NA, NH, KT V is VRA or VRR from volume scan	
20	AA, RA, NA, NR, KT V is VRA from fixed elevation scan	
21	RA, AA, ELM	Radial velocity at a point

22	R varying radar range within pulse volume DRR, RAZ, REL, BW	Mean radial velocity in radar beam cross-section
23	R, DRR, RAZ EL varying radar elevation angle within pulse volume BW	Mean radial velocity with respect to azimuth within pulse volume
24	R, AZ, EL Radar range, azimuth and elevation angle varying within pulse volume	Radial velocity at a point
25	X, Y, Z	U, V, W
26	X, Y, Z	U, V, W
27	ZP Array of heights values UP Matrix of headwind component VP Matrix of cross wind component WP Matrix of vertical wind component RP Array of horizontal distances along glide path NZ Number of heights NX Number of distances X, Y, Z	U, V, W

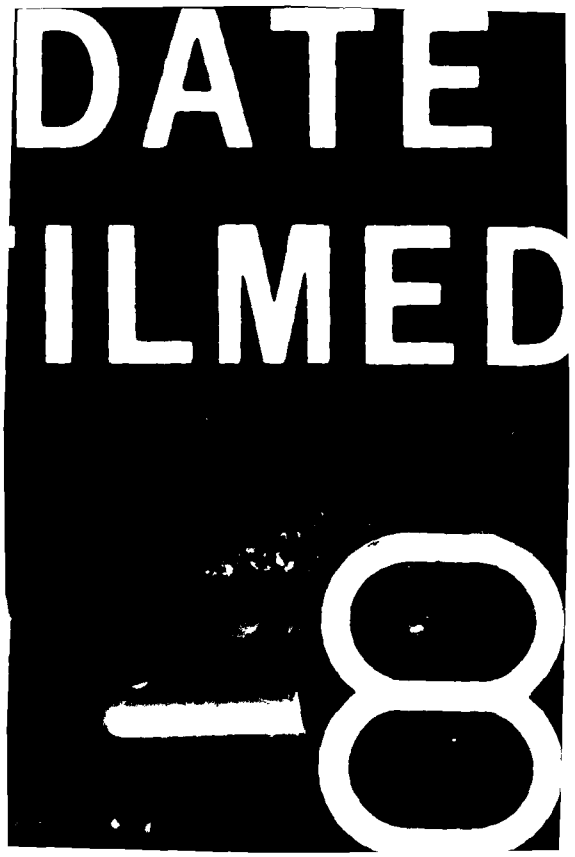
DATE
ILMED
8